

Department of Physics and Technology

# **Spectral measurement improvement through optical tree delineation.**

—  
**Jonas Toennis**

*FYS-3900 Master's thesis in physics 60 SP, Earth Observation*

*November 2017*





## Abstract

The development of miniaturized multispectral cameras that can be used on unmanned aerial vehicles (UAV) provide high resolution spectral data. The increase of flight height increases the areal covered, but reduces the resolution. While most UAV's fly at  $\sim 100$  meter, the data in this thesis was collected at 300 meter flight height, reducing the resolution. The lower resolution leads to a low resolution photometric surface, which is challenging to use in tree delineation without extensive ground knowledge. Optical delineation algorithms have successfully been used on satellite data of lower resolution than collected by the UAV, and can be translated to the UAV data. Three well established delineation algorithms were implemented for the optical tree delineation, Valley Following, Region Growing and Marker Controlled Watershed. The goal was to determine which of these three algorithms provides the fewest omissions while being general applicable across multiple tree species. A double Gaussian filtered Region Growing algorithms provided the best result towards that end.

The high resolution multispectral datasets over a large area take a long time to process and classify. By utilizing tree crown delineation, the elimination of data that is not a tree is possible, reducing the amount of processing required. A Support Vector Machine (SVM) was implemented to classify resulting data. While the traditional approach of using the entire pure tree stand in the classification resulted in an overall accuracy of 72% and a Kappa of 0.6345, isolating the tree crowns improved the classification to an overall accuracy of 80.3% and a Kappa of 0.7413, while decreasing processing time by 70%. Since a single tree crown should be a single species, all data belonging to the same tree crown was averaged, resulting in a single datapoint for each tree. This increased the classification to 81.6% with a Kappa of 0.7649.

Since the tree crowns are established, another factor that can be calculated from them is the standard deviation, both for products of the spectral bands, such as the NDVI, but also for each band individually. Since no attempt to use the standard deviation of the spectral reflectance in classification was found in the published literature, a classification based solely on the standard deviation of the tree crowns was attempted. The result gave an overall classification accuracy of 62.5% with a Kappa of 0.5186. This means that the standard deviation within a tree crown does contain species information, but whether that is a by-product of the sensors design, calibration error, or actual information is not clear. The addition of the standard variation to the mean spectral values increases the overall classification accuracy to 83.3% with a Kappa of 0.7860.



## Acknowledgement

The creation of this thesis has been a long process, and it would not have been possible without the support of of my friends, family and supervisors.

Firstly, I would like to thank my Supervisors Anthony Doulgeris and Corine Davids. Without your guidance, patients and flexibility in supervising this thesis, across an ocean and an eight hour time difference, it would not have been possible. While being busy, you where able to made time for hour long discussions, and for that I have to say : Thank you.

Thank you NORUT, for providing the data used in the thesis through the EU project North State (FP7 ref 606962). Especially thanks to Corine for calibrating, recalibrating and cutting of the datasets.

While not involved with the project i would also like to thank Björn Gustavsson, for teaching me two invaluable lessons concerning programming: 1) Be lazy, make ever code reusable and 2) Document everything so that you can be lazy later and reuse the code.

Jonas Toennis November 2017



# Contents

<b>1</b>	<b>Introduction</b>	<b>1</b>
1.1	Remote sensing in forestry . . . . .	1
1.2	Objective and Contribution: Spectral measurement improvement through optical tree delineation . . . . .	2
<b>2</b>	<b>Data types and tree delineation basics</b>	<b>5</b>
2.1	Data types . . . . .	5
2.1.1	Acquisition platforms . . . . .	5
2.1.2	LIDAR data . . . . .	6
2.1.3	Multi and hyper spectral data . . . . .	7
2.1.4	Photogrammetry . . . . .	8
2.1.5	LIDAR vs. Photogrammetry . . . . .	8
2.2	Basic tree crown delineation approaches . . . . .	9
2.2.1	Valley following delineation . . . . .	11
2.2.2	Region growth detection and delineation . . . . .	11
2.2.3	Watershed detection and delineation . . . . .	11
2.3	Recent work in delineation . . . . .	12
2.4	Pre-processing for forestry data . . . . .	13
2.5	Multispectral data and Tree-delineation . . . . .	13
<b>3</b>	<b>Study area</b>	<b>15</b>
3.1	Data Source . . . . .	15
3.2	UAV . . . . .	15
3.3	Cameras . . . . .	15
3.4	Area . . . . .	18
<b>4</b>	<b>Tree delineation implementation and modifications</b>	<b>21</b>
4.1	Valley following algorithm . . . . .	21
4.1.1	Valley following . . . . .	21
4.1.2	Rule based improvements . . . . .	22
4.1.3	Changes made to original algorithm . . . . .	22
4.1.4	Addition of 3D information . . . . .	24
4.2	Region Growing algorithm . . . . .	25
4.2.1	Adaption of original algorithm . . . . .	26
4.2.2	Addition of 3D information . . . . .	29
4.3	Marker Controlled Watershed . . . . .	30
4.3.1	Creation of the tree object . . . . .	30

## Contents

4.3.2	Marker generation . . . . .	30
4.3.3	Delineation of trees . . . . .	31
4.3.4	Adaption of original algorithm . . . . .	31
<b>5</b>	<b>Evaluon of tree delineation</b>	<b>33</b>
5.1	Valley following . . . . .	33
5.1.1	Blocking threshold . . . . .	33
5.1.2	Valley following results . . . . .	34
5.1.3	Application of SEM . . . . .	36
5.2	Region Growth . . . . .	36
5.2.1	Seed point generation . . . . .	36
5.2.2	Growth delineation results . . . . .	39
5.2.3	Application of SEM . . . . .	41
5.3	Marker controlled watershed . . . . .	41
5.4	Conclusion on Tree delineation and Spectral application . . . . .	42
5.4.1	Evaluation for spectral application . . . . .	44
<b>6</b>	<b>Methods and implementation of spectral investigation</b>	<b>47</b>
6.1	Use of Rikola Spectral data for delineation . . . . .	47
6.2	NDVI . . . . .	47
6.3	Automated classification . . . . .	49
6.4	Classification performance . . . . .	50
6.5	Species information in the standard deviation . . . . .	51
<b>7</b>	<b>Results of spectral investigation</b>	<b>53</b>
7.1	Rikola data for delineation . . . . .	53
7.2	Comparing spectral library values with measurements . . . . .	53
7.3	NDVI standard deviation improvement . . . . .	57
7.4	Automated classifier results . . . . .	58
7.5	Spectral Standard deviation . . . . .	60
7.6	Species information in the standard deviation . . . . .	62
<b>8</b>	<b>Discussion</b>	<b>65</b>
8.1	Rikola data for delineation . . . . .	65
8.2	The use of spectral libraries . . . . .	66
8.3	NDVI standard deviation . . . . .	66
8.4	Classification results . . . . .	67
8.4.1	Classification of Standard deviation . . . . .	69
<b>9</b>	<b>Conclusion and Remarks</b>	<b>73</b>
9.1	Future Work . . . . .	74

# List of Figures

2.1	Variation of Cannopy. Left: Variations between Pinus Mugo (90% of stand) and Larix sukaczwi(90% of stand) . Right: Canopy variations within a single species[42]. . . . .	10
3.1	Study area and UAV flight tracks. . . . .	16
3.2	Cryowing UAV and ground control systems. . . . .	16
3.3	Pure forest stands identified(from left to right): Birch(Betula pubescens), Siberian Larch(Larix sibirica), Pine, Silver Spruce(Picea glauca), Norway Spruce(Picea abis) . . . . .	19
3.4	Yellow is Birch, Blue is Larch, Light green is Spruce, Dark green is pine and red is sample area 1. . . . .	20
4.1	Center pixel is Valley material. O's are checked for additional valley material. left: Orginal implementation, arrow gives scan direction. right: adapted scanpattern and scandirection independent. . . . .	22
4.2	Merged trees with valley material giving in purple. left: Circles are crownareas where rules will split the trees. right: Circle marks a gap in valley material that is to large to result in a split. . . . .	23
4.3	Light green is changed valley matter. Circle: Removed matter for split, Square: Indentation removed, Diamond: Branches removed . . . . .	24
4.4	Four-way, linearly divergent search for radiometric maxima [8]. . . . .	25
4.5	left: Original workflow, right: Adapted and optimised workflow for Matlab	27
4.6	Improvement of maxima points . . . . .	28
4.7	Constraining network and the maxima points it is based on . . . . .	29
4.8	Gradient of illumination variation of closed forest cover. Left: Coniferous forest. Right: Mixed forest . . . . .	31
4.9	left:Watershed base on distance from treetop markers. Right: Watershed based on distance from Background markers. . . . .	32
5.1	Showcase of losing trees to thresholding. Circled areas are disappearing trees. Orange tinted area is a mixed tree stand. . . . .	33
5.2	Large Poplar trees overshadowing their neighbours due to the low sun angle.	34
5.3	Delineation through Valley following. Yellow: Manual outlined trees. Blue: Automated boundary. . . . .	35
5.4	Delineation boundaryes created by the Valley following with different filters. Left:Gaussian 3x3 $\sigma = 0.5$ . Middle:3x3 and 5x5, $\sigma = 0.5$ and 1. Right:3x3 and 7x7, $\sigma = 0.5$ and 1.5 . . . . .	36
5.5	Seed points before and after the intensity dip check has been performed. .	38

*List of Figures*

5.6	Seed points after the neighbourhood check for thresholds of 0.75 0.85 and 0.95 respectively. . . . .	40
5.7	Region growing with similarity thresholds at 0.65,0.75 and 0.85 respectively. Upper part of the images is a mixed forest stand, lower part is a coniferous stand. Yellow spots represent manually outline tree crown material. . . . .	41
5.8	Left: Averaged SEM 0.5 meter resolution. Right: Original SfM point cloud.	43
7.1	The delineation results for each band compared the Canon delineation. Red are tree crowns from Canon, Green are tree crowns from the Rikola bands. Overlap is yellow. . . . .	54
7.2	A clear offset between the two delineation results in the northern direction. Red are tree crowns from Canon, Green are tree crowns from the Rikola bands. Overlap is yellow. . . . .	54
7.3	Background error bar plots are showing the spectral values from SPECCHIO for the corresponding species. Each spectra line corresponds to the scaled resolution given in the legend in meters. . . . .	55
7.4	Showing the normalized reflection for Spruce(green) and Larch(black) for multiple sizes of tree crowns. . . . .	56
7.5	Spectrum plotted for each pixel identified to belong to the same tree crown. Seed is the thick black line. . . . .	56
7.6	The Ratio of the standard deviation of the single trees compared to the same resolution of the entire stand image. Below one is an improvement. left: Larch. right: Spruce. . . . .	57
7.7	The classification results based on the SVM classifier trained ton the tree crown averages. . . . .	61
7.8	The Ratio of the standard deviation of single trees compared to the same resolution of the entire stand image. Each line represents a Rikola band. Below 1 is an improvement. Top: Similarity measurement of 15%, resulting in well delineated tree crowns. Bottom: Similarity measurement of 5%, resulting in underestimated delineated tree crowns. . . . .	63
8.1	The reflectance values for Norway Spruce and Silver Spruce, where the Norway Spruce values are multiplied by a constant of 1.5 . . . . .	68
8.2	Top:The average over 20 mean tree reflectance spectra for each species. Bottom: The average over 20 standard deviations for the tree crowns of each species. . . . .	70

# 1 Introduction

## 1.1 Remote sensing in forestry

The use of remote sensing for forestry is well established. Satellites and plane imagery was used from early on for vegetation mapping. The normalized difference vegetation index was developed in 1974 [45] and is still in use today along with a number of other indices. The potential applications to forestry keep increasing with higher spatial and temporal resolutions.

Efficient forest management increases the demand for detailed, timely information. Information of forest parameters such as height, crown diameter, timber volume, growth rate and health have traditionally been collected on a stand basis by on site measurements of a few individuals. The rapid development of optical sensors increases the uses for forestry inventory. This gives the possibility to change out observation platforms such as planes and satellites, and substitute them with cost efficient, but coverage limited Unmanned Aerial Vehicles (UAVs) which are considered cheaper when focused over smaller areas [35]. The development in miniaturized hyper-spectral imaging technology makes it possible to fit multiple observation instruments on the same UAV which leads to multiple complementary data-sets.

For forestry applications, these datasets are usually still collected by plane, since the preferred combination of instruments is a multi/hyper spectral camera and a Light Detection And Ranging (LIDAR) instrument. The addition of tree height makes it possible to distinguish between species with similar spectral reflectance characteristics, but different mean heights [9]. With the addition of tree shape, roughness and other surface features, it is even possible to classify trees based on LIDAR measurements alone[41]. LIDAR is currently the golden standard when working with Digital Surface Models (DSM) of forest canopy with a full wave return showing both treetop, ground surface and other significant under canopy in one measurement. This feature of LIDAR makes it possible to create a Canopy Height Model (CHM) which is normalized to the terrain.

Photogrammetry, also called image matching, is a technique exploiting knowledge about camera positions and image overlap to calculate the distance to the imaged objects, thus creating a 3D surface. It can be created from aerial imagery in the processing stage of the data processing, and is as such easily available and providing additional information at a limited expense (computational time). The downside with Photogrammetry is that since it is based on a passive optical instrument, there is no wave return to detect other layers than the top layer. This means that photogrammetry shows only the forest canopy without providing information about the actual ground. In open canopies, where ground is visible, ground points between trees can be identified and exploited to

create a DSM in addition to the Surface Elevation model (SEM) resulting in comparable accuracy measurements as LIDAR[56]. There have been some studies working on application of photogrammetry, looking at a forests structural characteristics and a biotic damage [34] on both stand scale and tree scale [58]. The large downside in direct forest parameter estimation from photogrammetry is that in closed canopy situations, a DSM needs to be provided to create a hybrid CHM [33].

High resolution spectral measurements can provide us with details like tree species[9] and stress factors [40]. The spectral reflectance of a tree crown changes within the crown due to irradiation intensity [11], furthermore an average over multiple observations (pixels within the same crown) can reduce errors in the spectral measurements.

### 1.2 Objective and Contribution: Spectral measurement improvement through optical tree delineation

Automated tree crown delineation has been a well established area of forestry remote sensing. Algorithms developed for such purposes data back to the 90's [12]. Back then, these algorithms were developed for aerial and high resolution satellite imagery. Since then this field of study has had multiple high focus areas.

While passive optical imagery was at its peak in the 90's and early 00's, it is still a topic on which work is published. Improvements to algorithms are created, and long standing problems are solved in new and innovative ways, working with image object recognition and higher computational capacities available. Leckie et al. [27, 26, 28] is one of these that still works on improving delineation in high resolution imagery. Most optical tree delineation algorithms have been developed for specific forest areas or even tree species, and were based on a single band image analysis. With the increase in multispectral imaging sensors attempts have been made to expand tree delineation to multispectral imagery[54]. And while a few studies have been conducted in the area and they do show delineation capabilities, the published literature is limited.

Airborne LIDAR instruments created a complimentary dataset to the passive optical remote sensing datasets. Characteristic information on tree stand, and with high resolution, even tree level could be extracted. LIDAR became quickly the most used dataset in tree delineation. Being able to model both the ground and canopy at the same time, it gave information of height, as well as shape and texture of the tree[48]. The application of LIDAR is going to far as to not only provide additional information to spectral classification, but classification based on LIDAR data alone[41].

The current typical approach to areas where both LIDAR and Spectral datasets are available, is to delineate with the LIDAR data, and either refine the delineation through spectral data, or combine both datasets for classification[9].

With development of UAVs, very high resolution optical data has become easily available. While most UAV's currently are not suited for LIDAR data collection due to payload and power limitation, low weight cameras make optical data collection possible. Recent developments in multispectral imaging lead to cameras based on Fabry-Perot technology, greatly reducing the weight of multispectral imaging systems[38].

## 1.2 Objective and Contribution: Spectral measurement improvement through optical tree delineation

Higher computational power and higher resolution imagery lead to improvements in stereo photography techniques to the point where a moving digital camera could replace a multi lens sensor. By matching images from slightly different observation angles, a three dimensional model can be created (photogrammetry). Further improvement lead to a Structure from motion (SfM) algorithm, increasing the three dimensional modelling possibilities. High resolution three dimensional data is currently the most prevalent topic in delineation. In combination to the three dimensional data, the original images provide additional information and if a multi spectral camera was on the same flight as well, a comprehensive dataset is acquired. This dataset can be used for a range of functions, from simple tree delineation[38] to detection of stress factors[40].

The thesis looks into the little discussed area of high resolution (25 cm) UAV imagery applications. The resolution is a result of an increased flight height(300m) than average(<100m) to cover a larger area of interest, while still staying under cloud cover in comparison with satellite imagery. Specifically, this thesis looks into passive optical tree delineation methods and possible improvements through a 3D surface created through photogrammetry. It also looks into different preprocessing filters for tree delineation. Different tree delineation algorithms have been developed for different circumstances. Since the thesis explores any improvements in spectral measurements and possible detection of invasive species, the tree detection and delineation algorithms are evaluated against the fact that omissions are not acceptable, while a tree crown splitting is. Once the different tree detection and delineation algorithms have been evaluated, the spectral behaviour and classification possibilities are investigated. The goal is to measure any classification benefit by using tree crowns, rather than a traditional stand average as training data. This is especially relevant for open tree canopies with ground cover visible where a classifier might wrongly be trained with the entire image segment, and thus reducing classification accuracy. Additionally benefits that might arise as a result of the delineation are a reduction in computational time required for the classification as well as a better invasive species detection, since spectral values are not lost in the high resolution multispectral data or to the deviation arising from non targeted classifiers.

So the central questions that need to be answered for high flying UAV's are:

1. Which optical delineation method can be applied with the fewest omissions without specifying tree species?
2. How does a delineation impact processing time of the classification?
3. What effect does a delineation have on spectral data and species classification?

This thesis is organized as follows:

Chapter 2 An overview over widely available data types and algorithms

Chapter 3 Presentation of study area and available datasets

Chapter 4 Detailed implementation of tree delineation algorithm and modifications

*1 Introduction*

Chapter 5 Evaluation of tree delineation

Chapter 6 Methods and implementation of spectral investigation

Chapter 7 Results of spectral investigation

Chapter 8 Discussion

Chapter 9 Conclusion and remarks

## 2 Data types and tree delineation basics

### 2.1 Data types

There is a wide variety in sensors and platforms in remote sensing. While not all of them are applicable to forestry many of them can be used. The most used sensors for forest remote sensing are passive optical sensors like consumer grade, multispectral and hyperspectral cameras. The active sensors consist mainly of Synthetic Aperture Radar and Laser Scanning. While Synthetic Aperture Radar(SAR) is a useful instrument in estimating forest cover and biomass [22], I will omit it since my datasets do not include SAR data. Some SAR data applications are similar to Light detection and ranging(LIDAR) applications, giving range to target as well as secondary reflections, while other application use SAR data to estimate tree volumes and water contents.

#### 2.1.1 Acquisition platforms

There are three main platforms we can use: Satellites, Aerial vehicles and stationary observation platforms.

Polar orbiting satellites are very useful platforms with a wide range of instruments, many of them can be applied to forest observation. A polar orbit gives global coverage but is limited in the temporal resolution due to the repeat pass times. The temporal resolution can be increased by using multiple satellites with similar instruments and delayed orbits (Modis x 2, WorldView x 4) as well as with off nadir observation, removing the requirement to be directly above a target. The lack of illumination in polar regions during some seasons and cloud cover in general can make passive optical observations impossible. Further limiting factors are data acquisition rate, storage and downlink capacity. Landsat 8 has an acquisition rate of 384 MB/s [46], while IKONOS (0.8m resolution) has an acquisition rate of more than 500 MB/s.<sup>1</sup>

While medium (15-60m) and low(250 + m) resolution satellites (Landsat, Modis, Sentinel..) can be used for forest identification they cannot be used for tree delineation. They do however provide long standing data series to observe large scale changes. High resolution ( 0.5m resolution) satellites like WorldView have a panchromatic band at high ( 0.5m) resolution which can be used to improve the spectral bands resolution, which are collected at 1.2m resolution, in a process called pan sharpening[24].

Aerial vehicles divides into two sub divisions commonly referred to as planes and UAV's. Planes provide a larger payload capacity, on board surveillance of the instruments and larger areal coverage. Heigh operating costs and expensive camera equipment limits its availability, and minimum flight height affects the camera resolution. UAV's

---

<sup>1</sup>based upon coverage, resolution and bit-rate found in promotional material

## 2 Data types and tree delineation basics

are cheaper to operate, but have limited payload capacity and limited range. The different types of UAV's have different characteristics and best application areas. A Multiprop gyrocopter can provide large payload capacities[38] and could even accommodate stabilization equipment, it is limited in speed and coverage, but can provide a stable, unmoving image platform under the image collection phase. A fixed wing UAV can provide a higher speed and thus cover larger areas as well as providing higher flight altitudes. This increases the area coverage at expense of the resolution. Fixed wing UAV's are more sensitive to air currents and turbulence, which results in image blurring. Another large drawback on UAV's in general is the amount of time it takes to cover an area. With an acquisition time of one hour for my data, the changes in illumination can be significant due to cloud cover. Limited payload capacities are becoming less of a problem with lighter equipment which today allows us to fly multiple instruments at the same time on UAV's.

### 2.1.2 LIDAR data

A Light detection and ranging ,LIDAR, system is an instrument which measures distances by sending out a laser pulse and measuring the time until a return signal is received. The time interval is then transformed into spatial distance. Most modern LIDAR systems can detect multiple reflection returns from a single pulse. The first return is the reflection from the canopy. Since the canopy is not a solid continuous layer part of the laser pulse penetrates through it. The second return can either be scattering from underlying canopy structure such as lower branches or tree trunk, in which case the last return might signal ground, or it can be scattered by the ground. Due to the canopy being highly influential on the return signal, the differences of leaf on and leaf off measurements are drastically different. This is taking advantage of on deciduous forest where terrain mapping is flown in leaf off conditions to get the most ground contribution[44].

LIDAR's complexity depends on its use. A stationary device does not need more than a laser emitter-receiver scanning unit to measure distances from know points, while more mobile units used for forest observations from the air needs precise GPS and inertial measurement systems to co-locate the measurements.

Due to the geometry involved with the laser beam focus, the measurements can have large differences in both footprints and point density. CryoSat 2 is an example of a satellite with a LIDAR system on board and has a footprint of minimum  $0.5 \text{ km}^2$ . Airborne system have, with less distance to the ground, a higher resolution often varying between  $0.013 \text{ m}^2 - 0, 1 \text{ m}^2$ [50]. It is not only the size of the footprint that is important for the acquired data, but also the frequency of the acquisitions. The number of acquisitions is measured in points per square meter and ranges as example from 1.5 to 30 points per square meter in Vauhkonens *et al.* [50] comparison of delineation algorithms. In the study the acquisition platform for the data is not given, but acquisition height ranges from 130 meters (40 points/m) to 1200 m (1.5 points/m).

### 2.1.3 Multi and hyper spectral data

Passive optical remote sensing measures the amount of electromagnetic radiation reflected or emitted by the observed target. For measuring the reflected radiance, this method is heavily dependent on illuminating conditions where the main contributor is the sun. Different materials and attributes will change the reflection coefficients, which is measurable to an observer.

Multi and hyper spectral instruments are passive instruments that measure the radiance in a number of bands. A multispectral camera is considered as anything observing more than one wavelength, such that consumer cameras, which observe red, green and blue (RGB) imagery is counted in under multispectral observations. A much used modification for UAV observations is the removal of the infrared filter in consumer grade cameras (e.g. in the project North State) which results in an infrared/G/B sensor. Most spectrometers have somewhere around a dozen non-continuous electromagnetic bands. The bands and bandwidth depends on the application and instrument design. Landsat 8 has a multispectral instrument on board called the Operational Land Imager (OLI) which delivers 9 bands in the range of  $0.435 \mu m$  to  $2.294 \mu m$  in a non-continuous manner and at different resolutions, while the second instrument onboard, the thermal infrared sensor (TIRS) collects two bands from  $10.60 \mu m$  to  $12.51 \mu m$  [46]. Multispectral data is often used in ground type classifications such as the distinction between tree cover, bare soil, rock outcrop, natural pasture, degraded pasture and water bodies[51]. Other uses are ice surveillance, snow water equivalent calculations and more. The key to these application is a possibility to differentiate between ground types by having large differences in the spectral responses. Channels are usually specifically selected to increase the differences in reflectance.

Hyperspectral instruments are advanced multispectral instruments with a lot more bands, reduced spectral observation range per band and a continuous spectral coverage. These are often used for vegetation classification purpose. Dalponte *et al.*[9] does this with an airborne AISA Eagle sensor which measures 126 spectral bands, ranging from 400 to 990 nm with a spectral resolution of 4.5 nm . Dalponte *et al.* continued work with hyperspectral data varying the sensors and combining multiple Hyperspectral sensors such as the Hypspec VNIR-166 and Hypspec Swir-320i for a total of 307 bands ranging from 0.4 to  $1.7 \mu m$ [10]. It is worth pointing out that often a small sub set of bands from hyperspectral bands give enough information for classification purposes.

Spectral signals observed within a forest stand vary significantly. Some factors that contribute to the variations is non Lambertian scattering, canopy self-shadowing [19] and differences between the leaves in a single crown.

Due to the optics for optical data, the spatial resolution is highly dependent on the optics and range from target. Decreasing distance implies higher or easier to obtain spatial resolution.

Table 2.1: A summary of strengths and weaknesses of SfM from UAV[35]

Criterion	Strength	Weakness
Accuracy	Performs well over bare ground.	Performs poorly with poor image coverage.
Cost	Cost-effective for small areas. Cheap hobbyist UAVs available (e.g., the one used in [16]). Open source SfM/MVS software available.	Open source might not be as accurate as commercial software. Cheap camera models (e.g., GoPro) introduce large distortions in SfM models.
Ease of use/Learning curve	Full autonomous missions. Automated data processing.	Post-processing still requires experienced users.
Amount of data	High density point clouds. Easy interpretation of point cloud because of true colour rendering.	Classification of points based only on point height (no return number).

### 2.1.4 Photogrammetry

Photogrammetry is based on the basic tenets that 3D structures can be resolved from a series of overlapping offset images with different view angles. The result is a surface model with a varying point density based upon marker point correlation between images [35]. This usually works by knowing the camera orientation and positions, thus working out the geometry based on a network of targets with known position. Recent progression automates these processes by using highly redundant, iterative bundle adjustment based on a database of features automatically extracted from a set of multiple overlapping images. The bundle adjustment is an improvement over factorization when there are parts of the data missing. However, bundle adjustment has no direct solution and is quite slow for processing scenes with a large number of images [47]. Structure-from-Motion(SfM) is a photogrammetry method that does not need to use camera positions as input, but it needs a manual alignment to the real world[53]. While the camera position is not required for the SfM it can be used to decrease computation time. A comparison evaluation done by Westoby *et al.*[53] between LIDAR and SfM photogrammetry shows that 94% of all points lie within  $\pm 1$  m with 86% being between  $\pm 0.5$ - $0.5$ - $0.5$ m. Most of the variation in the difference is the result of dense shrub and bush cover. 100% of all cells without vegetation fall into  $\pm 0.5$  m range.

Mlambo *et al.* [35] sums up the properties of UAV photogrammetry well in Table 2.1.

### 2.1.5 LIDAR vs. Photogrammetry

Both LIDAR and Photogrammetry can provide us with a Surface elevation model (SEM), but only LIDAR can provide us directly with a viable Canopy Height model(CHM). For a CHM based on Photogrammetry a Digital elevation model (DEM) needs to be known beforehand in dense forest, while in an open canopy cover (<50%) the amount of ground points is high enough to be viable on its own [35].

The comparison between LIDAR or Airborne laser scanning(ALS) and photogrammetry is limited in the literature. There are some studies that compare datasets over

the same areas against each other, but only under either specific circumstances or with different resolutions. A paper by Murphy *et al.* [37] published in 2008 goes so far as to claim that LIDAR DEM models have far greater spatial resolution than photogrammetry. This might have been true in 2008, but is completely invalid in 2017. The progression of image systems can create DEM models with a far higher resolution. The WordView photogrammetric DEM model has been created with a 2 m resolution over larger areas [1] which to be fair is on the low end resolution compared with LIDAR's 1.5 to 30 points per  $m^2$  collected by air-borne systems. However UAV's have changed the situation by making it possible to access high resolution data for an area from which to construct a more detailed SEM model. The DEM model used later in this thesis is created by an UAV, with a 50-cm resolution or 4 points per  $m^2$ . Higher resolution can be achieved based upon the spatial pixel resolution before processing. Based on the values found in a number of papers, the spatial SEM resolution seems to be a third to a half of the optical image resolution

A validation study done by Chang *et al.* [6] in 2004 looks at the accuracy of DEM models when compared to Real-Time Kinematic (RTK) GPS. But also, here the photogrammetric DEM model has a large resolution (30m), while the ALS gives up to two points per  $m^2$  with a triangulation to a 5 m DEM model. The results show that ALS has the best accuracy with 0.09 m to 0.3 m and a photogrammetric accuracy of 1.03 m to 3.75 m [6].

Mlambo *et al.*[35] evaluates Photogrammetry against LIDAR data on similar resolutions (LIDAR 1 point/ $m^2$ , SfM 2 - 3.3 points/ $m^2$ ). They find a strong correlation ( $R^2=0.75$ ) with an average of -0.03 m and standard deviation of 2.38 m in one of their study sites.

Other published literature found with the same or similar resolution doing a comparison of Photogrammetry and LIDAR data found was done by Adams[3] with imagery from 1976. While having convincing arguments for a relative small change of topography and a high resolution (16 cm/pixel resulting in 2m DEM) all his photogrammetry results do have a negative mean discrepancy. He concludes with a rms error of 0.26 m for LIDAR and 0.43 m for photogrammetry[3].

## 2.2 Basic tree crown delineation approaches

High resolution remote sensing is a valuable tool for quantifying the distribution and density of trees with applications ranging from forest inventory and mapping urban parklands to detecting change[51] within tree stands [40]. The work of interpreting aerial photography has been dominated by human interpreters focusing on RGB images with the help of stereo-photography. This approach is useful for forest inventory on a larger scale (e.g. stands). While it can give details about stands, their extent and to a part also the species composition, the result depends on the human interpreter. As such, estimates of forest parameters can vary between interpreters.

An early application for digital analysis of aerial forest images were to get computers to outline the tree stands. These were then compared to human interpretation. The

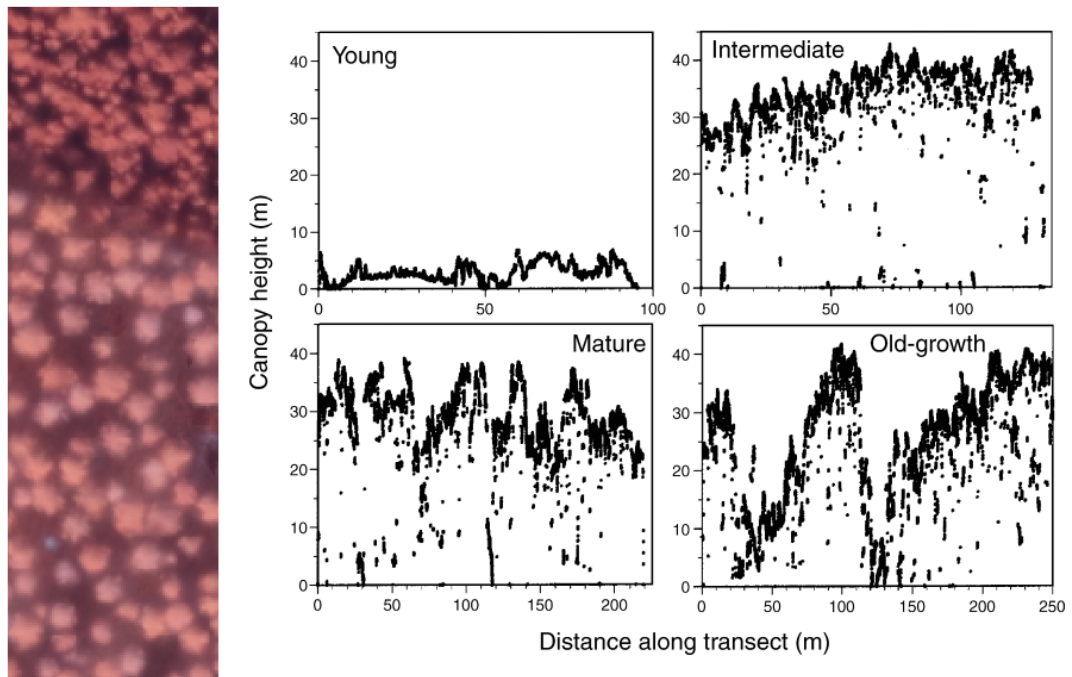


Figure 2.1: Variation of Canopy. Left: Variations between *Pinus Mugo* (90% of stand) and *Larix sukaczwi* (90% of stand). Right: Canopy variations within a single species [42].

stand is the typical forester unit for an area of trees with the same properties.

Forest stands can be either managed or natural. A managed stand goes under forest plantation and is usually highly controlled and the characteristics well known. Plantation stands are often planted at the same time and consisting of a single species. Natural stands are unmanaged, and often of a mixed composition where tree species is dependent on the environmental characteristics [57]. Due to not being actively managed, the stand characteristics will vary more and result in a more complex canopy.

The complexity of the stands does increase uncertainties in the extrapolated averaged measurements like crown diameter, age, health and wood-volume.

The distinction between tree crown detection algorithms and delineation algorithms is not always clear, and the region growth is one algorithm that makes use of the detection to create the delineation. As such definitions tend to deviate, resulting in the more general term of "detection and delineation" methods [20]. Going forward, I'll refer to delineation for the outlining of tree crowns either direct or through a derivative from treetops, while detection will be used where treetops are found and marked.

A wide variety of detection and delineation algorithms have been developed to separate individual trees. The large variations within canopy structure of varying species (image in figure 2.1) and even within a single species (graphs in figure 2.1) makes it difficult to clearly separate individual trees based upon a limited number of parameters.

### 2.2.1 Valley following delineation

One of the early algorithms that is still used today [28, 26, 27] was created by Gougeon[12] in 1995. The algorithm works on single band intensity, and uses a geographical valley-following approach. The algorithm is divided into two processes. The first is to find the local minimum points in the images intensity, and follow the shaded area around the trees. The second step after the valley following is complete is the clockwise based outlining of the trees based upon a set of predefined rules that look for tree gaps and tree fusions. This was done with MEIS-II optical imagery at 31 cm resolution. The results of this automated tree count based on the study areas of coniferous trees outlined 1189 trees out of a ground count of 1288 (92.3%) The manual outlining in photographs resulted in 1179 and 1046 tree crowns (91,5 % and 81.9% of ground count). Where both manual and automated tree crowns were marked, 81 % of them had a good fit [12].

### 2.2.2 Region growth detection and delineation

Region growth was introduced by Culvenor in 2002[8]. He based his algorithm on a single channel NIR due to its ability to accentuate the shadows between trees. The algorithm starts from the treetops and is based upon the local maxima and local minima to cluster the crown pixels. The maxima are used to calculate the seed points which should correspond to the treetops. The local minima are combined to create a constraining space. The pixels around the seed are then included in the tree crown if they are over a brightness threshold based upon the seed brightness, do not cross the constraining space or belong to another already classified crown. Due to the brightness constrained in the growth phase, the algorithm starts with the brightest seeds. Culvenor developed and tested the algorithm on Eucalypt forests. With 356 trees in the image the algorithm found 354 clusters but he also points out that not all clusters were trees.

### 2.2.3 Watershed detection and delineation

The watershed algorithm detects drainage basins where water would flow in a topographical landscape. This topographical landscape is created using the intensity levels of images, and is thus a single band algorithm. By inverting the forest images, the tree tops will have the lowest values and can thus be used. This can be used on single band data as well as multispectral data [54]. The watershed algorithm is prone to a large amount of noise and over segmentation [20] consequently estimating far more and smaller tree crowns. The noise and the application to closed shaped objects as found in deciduous forest led to quick improvements once the application of the algorithm to forest canopies was used[52], resulting in a marker controlled watershed algorithm. The constructed markers limit the amount of allowed basins. How the markers are created varies. Some base them on crown radius [23] while others base the markers on edge detection between the background and obvious trees [52]. By using a spectral angle Yang [54] reached accuracies of up to 90%.

### 2.3 Recent work in delineation

The improvement of delineation algorithms is ongoing work. The problem with improvement of delineation algorithms is that there is a large spread in both application area and dataset compositions. The most used tree type to evaluate delineation work is (mature) Norway spruce because it is a round distinct shape in a nadir angle. This means that a lot of algorithms break down when exposed to mixed forest types. The number of studies done to actually address the comparison issue between algorithms are limited, and as such we mostly talk about improving on a single algorithm without comparing it with others. Ke [20] tried to compare the earlier presented three algorithms on the same datasets. His conclusions were that all algorithms showed the ability to effectively delineate Norway spruce tree crowns based on a single band image (green). However, when presented with irregular tree crowns from hardwood the algorithm's basic assumptions broke down. He concludes that the region growing algorithm gives the best accuracies overall, partly because it does not make assumptions of the crown shape and has a higher tolerance of within class variation in hardwood crown reflections.

Leckie *et al.*[28] is using the Valley-following algorithm as a basis for further crown delineations. In the article series he describes criteria for re-evaluation of valley following results. Discussing remedies for the valley-following algorithm for mergers [27] and splits [26] using an evidence based rules approach. He investigates different possibilities of identifying and processing the incorrectly delineated trees, and finds that the accuracy improvements vary depending on pre tree shape and methods used for breaks and splits.

Novotny *et al.*[39] tries to improve the region growing algorithm by applying an adaptive histogram equalization and Voronoi diagrams to limit the growth. While he gets results for the delineation, he does not compare it to the original algorithm on the same images, and is thus not showing any proof of the improvement. Additionally, his evaluation of the delineation is unique when compared with other papers, using a 4 step overlapping system.

Barnes *et al* [4] investigates the improvements for region growth and marker controlled watershed algorithms based upon LIDAR data. He investigates multiple resolution and pre-processing methods to improve tree delineation for diseased larch forests. Trees under heavy attack will lose foliage, which leads to data pits, which complicates the tree crown delineation for crown deterioration assessment. He concludes that the absence of an optimal method for the use of Canopy height models for tree crown delineation across multiple study sites highlights the difficulties in applying a single algorithm. His pit removal does also not consistently outperform the standard canopy height model, but he does point out that the marker-controlled watershed demonstrated a superior performance.

Novotny[39] works with the region growing algorithm. He starts with a hyperspectral datasets from which he selects 7 bands that show spectral vegetation characteristics and averages them. He then applies an adaptive histogram equalization based upon a pixels neighbourhood to increase the contrast in the image and highlight shaded crown parts. Improvement of delineation is a still ongoing topic with new suggestions and studies appearing regularly. The neighbourhood size is crucial in these calculations and should

correspond with the expected crown size and is thus resolution dependent. After the adaptive equalization and a low pass filter to remove the crown details, the maxima were identified and evaluated if they were indeed tree crowns [16]. Starting from all the local seed points simultaneously and growing the regions in equivalent steps until a significant boundary is encountered. The algorithm was tested on 80 cm resolution multispectral imagery of Norway Spruce. The detection of treetops were between 78 and 84 % accurate while the crown outline was only 52 to 64% correct compared to manual outlining[39].

## 2.4 Pre-processing for forestry data

The subject of dataset pre-processing before delineation is often omitted in studies, or simplified to: an average filter was applied. There are some studies that go into detail about the implications and changes to results that come from pre-processing. One of these is by Chen [7] in which he works with small footprint LIDAR data. He points out that errors increase when the filter size grow larger than the trees, since it reduces the valleys between trees. At the same time, a filter needs to be large enough to cover most of a tree to only give one treetop. Ke [21] points out the same and uses a shape based template matching to remove the multiple maxima within a tree. Wang [52] uses the same reasoning for multispectral data.

## 2.5 Multispectral data and Tree-delineation

Hypers-spectral data carries with it a lot of information. Nasa's Airborn Visible/Infrared Imaging Spectrometer (AVIRIS) is a airborne sensor system providing a total of 224 bands at a resolution of 2 to 20 meters dependent on flight height. The use of a large dataset is computational heavy, and a smaller subset of data can provide the same results as long as the used bands are carefully selected. It is not uncommon for studies to select a subset of available bands corresponding to other sensor system for comparisons.

The idea of using spectral data on delineated trees is not new, and has been done before. One of these examples is published by Heinzl *et al.* [15]. His tree delineation is based on the LIDAR CHM model with resolutions from 0.3 to 1 meter. Once the Crown boundaries are found, a colour infrared (CIR) image is used to see if the vegetation within each crown boundary is the same. If not, the crowns are split based on the CIR data and the trees are classified out form a subset of possible trees.

In a later publication Heinzl *et al.* [14] goes further and uses LIDAR features such as LIDAR waveforms, height and texture in combination with with a 125 band hyperspectral image to classify species on a 1 meter grid. Said grid is then overlaid on a tree delineation, and split according to the species data.

Nevalainen *et al.* [38] also uses 3D data created through SfM to create the delineation. I am approaching the subject from the opposite direction, using the passive optical observation of the infrared band to delineate the trees, before classification. This is

## *2 Data types and tree delineation basics*

due to the higher resolution of the optical data, as well as the possibility to reduce computational cost by not computing a SfM surface for the area.

## 3 Study area

### 3.1 Data Source

The data for this thesis is provided to me by NORUT through the EU funded project North State ID number: 606962. North State was a project run from September 2013 to January 2017 and investigated the carbon and water balance modelling of Northern Forest Ecosystems. The data collected for the project consisted of Satellite data (Sentinel 1/2 and Landsat) and UAV data.

While North state UAV data covered three different regions (South and North Finland and Iceland ), I'll focus on the UAV data data collected in Iceland in the summer of 2015 (figure 3.1).

### 3.2 UAV

The UAV covering my study areas was a Cryowing Scout developed by NORUT and based on the ET-Air Cruiser Mini Airframe. It is a twin engine design, with its main batteries distributed in the wings. This allows for a large payload bay in the fuselage. It can carry a payload of up to two kilos (excluding batteries) and has a flight speed of about 20 m/s but is dependent on the current wind speeds. Image and specification of the Cryowing are figure 3.2 and *table 3.1* respectively.

### 3.3 Cameras

The payload on board when the data was collected was a Rikola Hyperspectral Camera produced by Rikola LTD in Oulu, Finland and a NDVI Camera based upon a consumer

Table 3.1: Cryowing Scout specifications

Weight	8 kg maximum take of weight
Wingspan	2.7 m
Ground Equipment	PC with 433 MHz radio and tracking antenna (5-10 km range)
Flight	Automatic (FPS based pre-programmed track, but under ground control, catapult launch, belly landing)
Range	90 minutes or 80 - 100 km, depending of wind and batteries
Payload	Rikola Hyperspectral Camera and 12 Mpx NDVI camera

### 3 Study area



Figure 3.1: Study area and UAV flight tracks.



Figure 3.2: Crywing UAV and ground control systems.

Table 3.2: Rikola Hyperspectral Camera specifications

PARAMETER	SPECIFIED VALUE	REMARKS
Horizontal FOV	> 37°	
Vertical FOV	> 37°	
Default Spectral Range	500-900 nm	Spectral range can be selected from range 400-950 nm with <u>long and short pass filters</u>
Min Spectral Resolution	10 nm, FWHM	For a high spectral resolution the spectral range needs to be limited.
Spectral Step	< 1 nm	
F-number	~2,8	
Image Sensor	CMV4000	CMOSIS CMOS image sensor with 5.5 $\mu\text{m}$ x 5.5 $\mu\text{m}$ pixels.
Image Sensor Pixel Clock Frequency	80 Megapixels/s	Readout of the whole 4 megapixel image takes 25 ms
Default Spectral Image Dimensions	1024 x 1024 pixels	
Max Spectral Image Dimensions	1024 x 1024 pixels	
Weight	< 700g	
Main Dimensions	80 mm x 97 mm x 159 mm	

Canon Powershot and modified by MaxMax.

The Rikola hyperspectral camera collects a single spectral band at a time with a spectral width of about 10-15 nm. While connected to a computer, the camera can collect an unlimited number of spectral bands, but is limited to 15 bands without a computer connection. A single band acquisition takes about 100ms whereof 15 ms where used for the observation, and the rest for saving and readjustments. Which results in an image acquisition time of 1.5 - 2 s. This is not a problem for a stationary camera, but in our case, mounted on a UAV moving at approximately 20  $\text{m s}^{-1}$  the observation points changes by up to 40 meters while collecting the 15 bands for an image. This spatial offset needs to be corrected in the final images. Further, the variable lighting conditions due to cloud covers makes a radiometric correction challenging. The Rikola camera specifications can be found in *table 3.2* and the chosen bands and their bandwidth in *table 3.3*.

The NDVI camera is based on the consumer camera Canon Powershot. The modification was done by changing the red filter with a NIR filter. This changes the band centre-points towards the 720 nm range and reduces the band width considerably in comparison with a normal red filter. This means that in this case, the NDVI needs to be based on the blue band instead of the red. This means that the NDVI is more sensitive to the distance to target due to Rayleigh scattering.

Table 3.3: Rikola bands collected

Band	Wavelength	FWHM(nm)
1	501.96	9.8
2	529.51	15.57
3	560.07	9.5
4	568.23	13.65
5	645.37	12.51
6	665.62	14.26
7	706.15	14.34
8	726.02	14.47
9	740.34	14.98
10	756.44	14.81
11	774.59	13.92
12	782.64	14.13
13	839.85	14.16
14	857.35	14.78
15	866.69	15.94

### 3.4 Area

The data collection was conducted in Iceland of the Hallormstadir forest (65.13 lat - 14.69 lon), August 24th 2015. The time and place correspond to a solar illumination angle between 30 and 35 degrees from 10 am to 10 pm.

The images were acquired every 50 meters at a flight height of 300 meters. This resulted in large overlaps of 70 % along track and 60 % across tracks for the Rikola images and even higher overlap for the NDVI camera which has a higher field of view. The NDVI images were orthomosaic through Agisoft Photoscan. The same program was used to create the SEM point cloud.

The data from the Rikola camera needed more adjustments. Due to the camera only collecting one band at a time, all of the bands have spatial offsets from each other. The images also needed to be radiometric corrected. The complete process of the Rikola image processing can be found in the works of Honkavaara [2]. The Rikola Camera was calibrated at ground, and due to changes in illumination during the flights the reflectance values range from 0 to 180 % instead of 0 to 100%. The NDVI image was rescaled to 25 cm resolutions, while the point cloud created from the same images was averaged to a 50 cm SEM model.

Five pure forest stands were identified. These are **Picea glauca**(White Spruce) covering a 6100 m<sup>2</sup> area, **Larix sibirica**, Siberian Larch, covering a 9700 m<sup>2</sup> area, **Betula pubescens**(Birch) covering a 6100 m<sup>2</sup> area, **Picea abies**(Norway Spruce) covering a 6100 m<sup>2</sup> area and a Pine stand covering a 2000 m<sup>2</sup> area. Their locations can be seen in figure 3.4.



Figure 3.3: Pure forest stands identified (from left to right): Birch (*Betula pubescens*), Siberian Larch (*Larix sibirica*), Pine, Silver Spruce (*Picea glauca*), Norway Spruce (*Picea abies*)

### 3 Study area

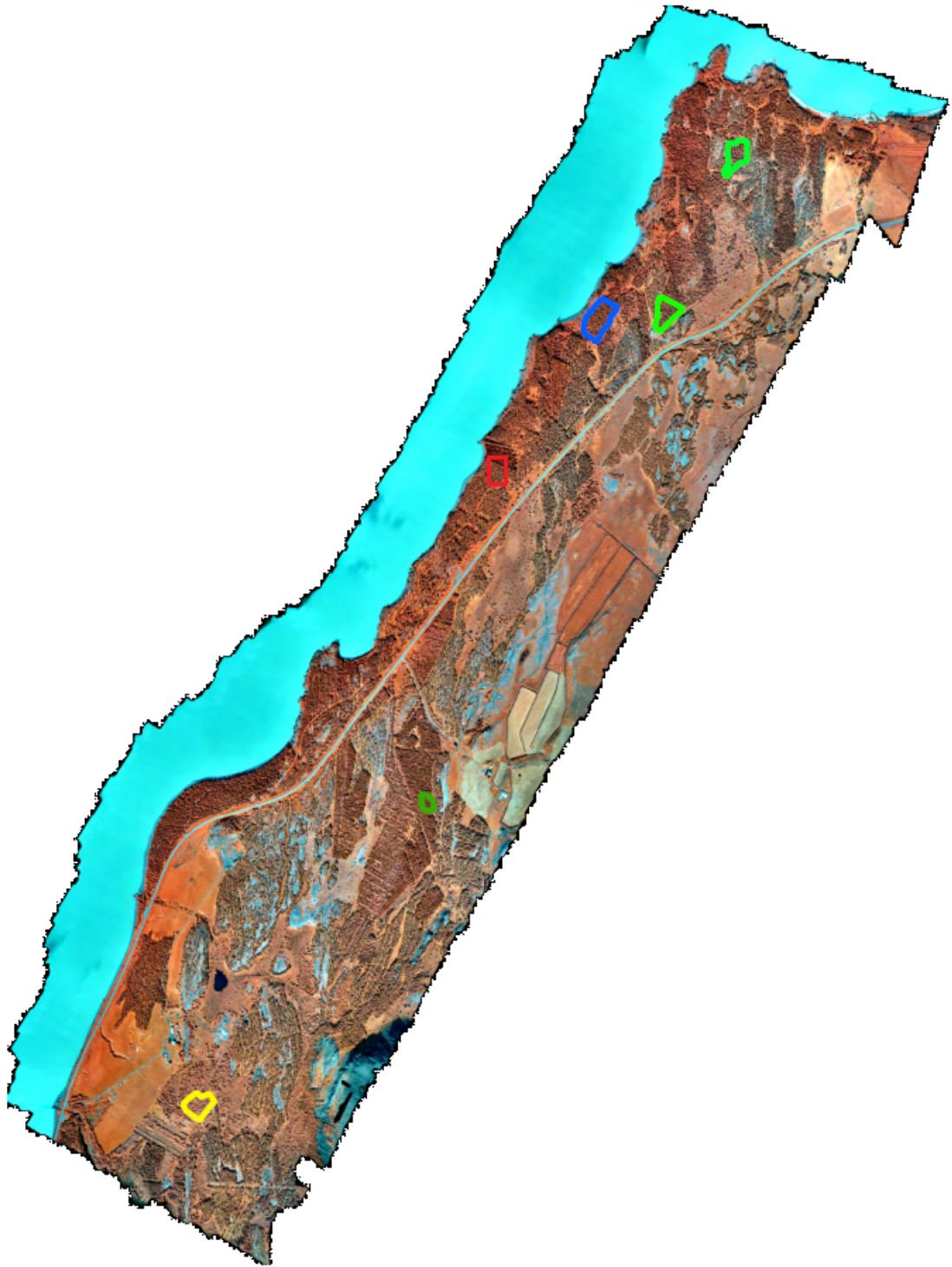


Figure 3.4: Yellow is Birch, Blue is Larch, Light green is Spruce, Dark green is pine and red is sample area 1.

## 4 Tree delineation implementation and modifications

### 4.1 Valley following algorithm

Valley following, first introduced by Gougeon [12], is based upon the fact that a tree crown will have a larger reflection than the shaded area around it. This can be represented as a topographical landscape where the single band reflectance is considered as height. In theory, by following the shaded, low reflection area one would be left with bright objects that would be tree crowns. While this assumption holds true in not too dense coniferous forests with their conical shape, it does not hold equally well for deciduous forests, forests with complex canopies or image acquisitions with a large observation angle. To reduce the delineation based upon the valleys, Gougeon devised a set of rules that work to counteract artificial indentation into tree crowns as well as splits trees that are only connected by a small amount of valley matter. The clockwise assumption of the rules does however assume that the tree crowns are closed and in a clockwise traceable shape. While the algorithm can split trees, it can not merge them, and is as such prone to oversegmentation.

#### 4.1.1 Valley following

The algorithm starts out by classifying all pixels below a set threshold to belong to the valley class. This value is set such that it is enough to block canopy gaps without removing too many shaded crowns. The value is chosen manually, and varies between images dependent on the forest type and complexity as well as illumination. Once the threshold is found the algorithm looks for local minimum points in the remaining image and adds them to the already valley marked pixels from the threshold.

Based upon the initial valley pixels a scan is initiated from the upper left corner towards the lower right corner. When the scan finds a pixel marked as valley material it extracts the neighbourhood and checks its immediate neighbours (O's in left side of figure 4.1) in the scandirection if they are flanked by higher values or not. If they are, then the pixels are set to valley material. In the same manner, two and three pixel wide valleys are considered. Once the scan has finished, the scandirection changes with 90 degrees. The scanning and change of scan direction continuous until four consecutive scans do not add any new valley material.

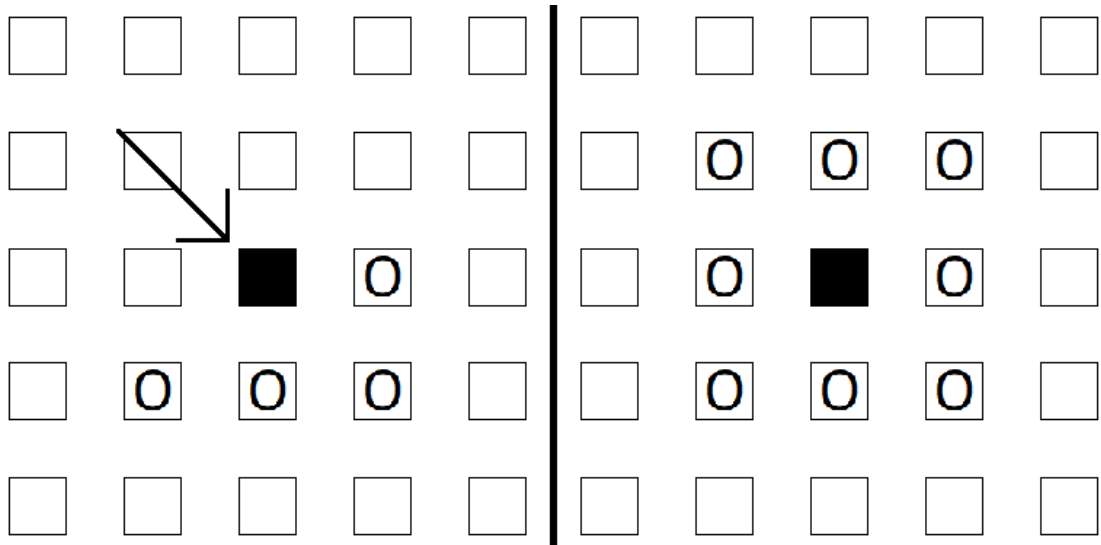


Figure 4.1: Center pixel is Valley material. O's are checked for additional valley material. left: Original implementation, arrow gives scan direction. right: adapted scanpattern and scandirection independent.

#### 4.1.2 Rule based improvements

After running the valley following algorithm, there is need for remediation due to crown merging as seen in figure 4.2 where the valley material does not surround the individual trees. The rules set forth by Gougeon focus on splitting joined tree crowns. The similar resolution (31 vs 25 cm) leads to the assumption that the rules can be applied straight forward without needing to modify them based upon resolution differences. As such, the rules start at the left side of the tree, and trace it clockwise, checking under way if additional valley material need to be added for splitting crowns(Circle in figure 4.3), or if it encounters a 180 °turn it removes valley material to remove the indentation in the tree crown(rectangle in figure 4.3) It can also remove single branches or outlying structures outside of the tree crown(diamonds in figure 4.3). Due to the way the algorithm is implemented it only splits trees that have less than 3 pixels of valley material connecting each other. The circles in the left image of figure 4.2 mark situations where a split will happen, while the right image of the same figure shows a circle where the gap in valley material is to large too qualify for a split (larger than three pixels)

There are some crowns that are split by the valley following but since the rules are based upon the binary Valley mask it is not possible to remedy it by a simple set of rules.

#### 4.1.3 Changes made to original algorithm

When implementing the algorithm, I made a few changes. I changed the valley following scan from a directional based scan(see figure 4.1 left) to a circular scan(see figure 4.1

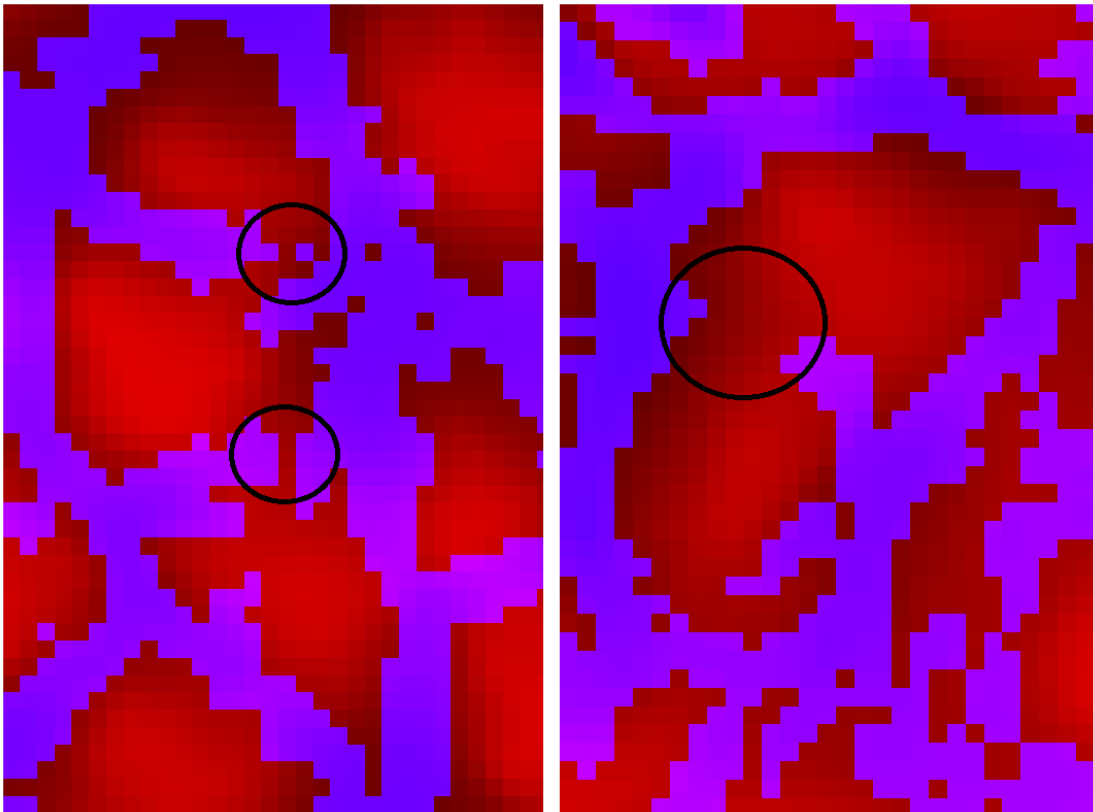


Figure 4.2: Merged trees with valley material giving in purple. left: Circles are crown areas where rules will split the trees. right: Circle marks a gap in valley material that is too large to result in a split.

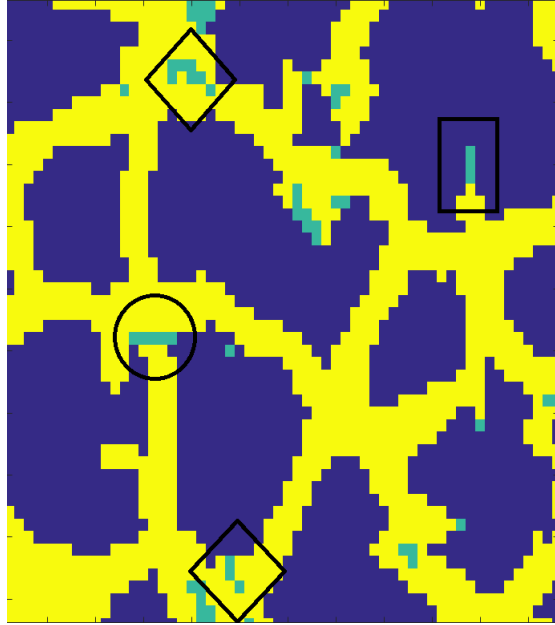


Figure 4.3: Light green is changed valley matter. Circle: Removed matter for split, Square: Indentation removed, Diamond: Branches removed

right), reducing computation time. This reduces the number of iterations needed to reach a stable result and removes valley tendencies in scan directions. I implemented a maximum iteration limit. This is set to 50, which is twice as much as most of my samples needed. One sample managed to hit the limit regularly, but showed only single pixel changes. At that point, the computational cost is simply too high to continue. I also changed the rules slightly to allow larger turns in earlier rules. This was a change that needed to be made to reduce the number of edge case errors and consists of a  $90^\circ$  right turn on Rules Level 1, where Gougeon only suggests allowing a  $45^\circ$  right turn.

#### 4.1.4 Addition of 3D information

Since the algorithm interprets the intensity value as terrain where the intensity is used as height, it can be assumed that the same algorithm will work with the 3D surface extracted from the photogrammetry. Larger terrain variation should not interfere with the results since the algorithm works with a limited neighbourhood and does not apply global constant. The change made to the algorithm is the removal of the valley threshold since it is useless in this application without a CHM which I do not have.. A linear interpolation from our 50 cm SEM data is used to compare the results.

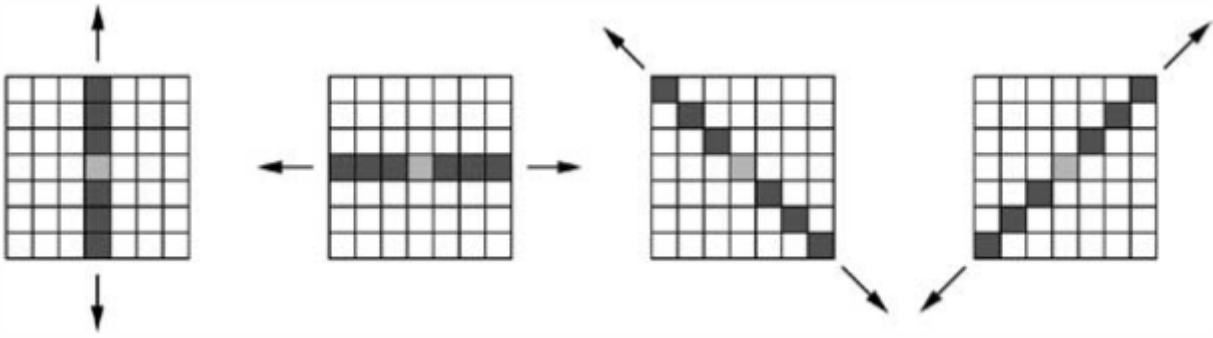


Figure 4.4: Four-way, linearly divergent search for radiometric maxima [8].

## 4.2 Region Growing algorithm

This is a tree identification and delineation algorithm designed by Culvenor in 2002 [8] to automatically delineate trees in high spatial resolution imagery. It is also based on the assumption that the irradiance of treetops is the highest due to the typical convex shape of a crown which leads to a directly illuminated area and therefore higher irradiance at varying sun angles. In denser forests the self-shadowing effect (shadow from other treetops will block or reduce the irradiance from lower parts of the tree) and will make this behaviour more observable. Selfshadowing increases with decrease of the sun angle. This irradiance behaviour means that geometric profile and the radiometric profile of a tree crown can be assumed similar and thus used for tree delineation.

The Region Growing algorithm follows a three step process:

1. Identification of local maxima throughout the image.
2. Identification of local minima throughout the image.
3. Clustering of crown pixels.

### Identifying local maxima

The local maxima are used to identify a treetop. As such it is important to find a single well placed maxima which then is used as a seed point to grow the clusters in step three. Culvenor solved this issue by stepping away from a user defined neighbourhood and uses 4 length unlimited scan directions anchored on a single pixel instead (*Figure 4.4*). The number of times that each pixel is identified as a local maxima is recorded, and the results, ranging from 0 to 4, indicate the probability of the point being a tree top. The addition of more search directions did not improve the identification process significantly [8]. Culvenor identifies the pixel as maxima when each of the opposing directions are lower than the central pixel, and at least one of the arms start rising again after an unspecified and unlimited length.

He points out that the seed points assignment needs to be evaluated by a human, and the decision on where to set the threshold for accepting a seed based upon the number of maxima identifications from the scanning is dependent on the complexity of the forest canopy.

### Identifying local minima

The local minima are used to create a constraining network to limit the clustering. As such they should encircle single trees. The evaluation method for minima is very similar to the maximum evaluation. It is still a four direction, unlimited search (*Figure 4.4*). However, a minima only needs to be classified once, and is accepted as such immediately. A minima is defined if both arms are greater than the centre and at least one of them decreases again. Due to the unlimited nature of the searches a point can be classified as both maxima and minima. In these cases the minimum takes precedence. Once the search is done, the constraining network (looking similar to the results of Gougeon 4.2) is refined as follows:

1. Closing gaps in the constraining network
2. Removing "dead end" boundary pixels
3. Reduce the network width to a single pixel.

### Clustering of pixels

The clustering grows the seed to surrounding pixels if they fulfil a similarity condition. The similarity condition is designed such that the pixels added to the seed belong to the tree crown. Culvenor defines the checked pixel to belong to the tree crown when:

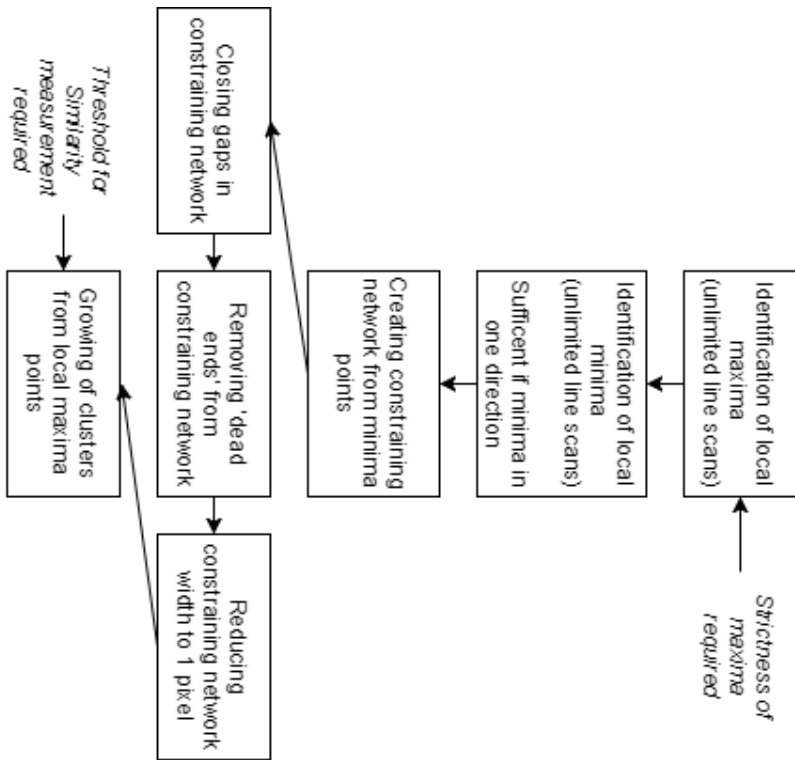
- brightness of pixel  $\geq$  (*seed \* threshold*)
- pixel does not belong to constraining network
- pixel does not belong to another crown

The brightness limitation makes the order of processing of seed points significant since a low value seed will envelope a larger area. As such the process starts at the brightest seed. Even so, some cluster merging can appear, which is the reason for a non-overlapping definition (bullet point three).

#### 4.2.1 Adaption of original algorithm

The changes made to the original algorithm are many. This is not a criticism of the original algorithm. The original algorithm (programmed in C++) would have been computational challenging in Matlab. As such, extensive changes have been made to reduce computational time, while obtaining similar results.

### Original Region Growing Algorithm



### Adapted Region Growing Algorithm

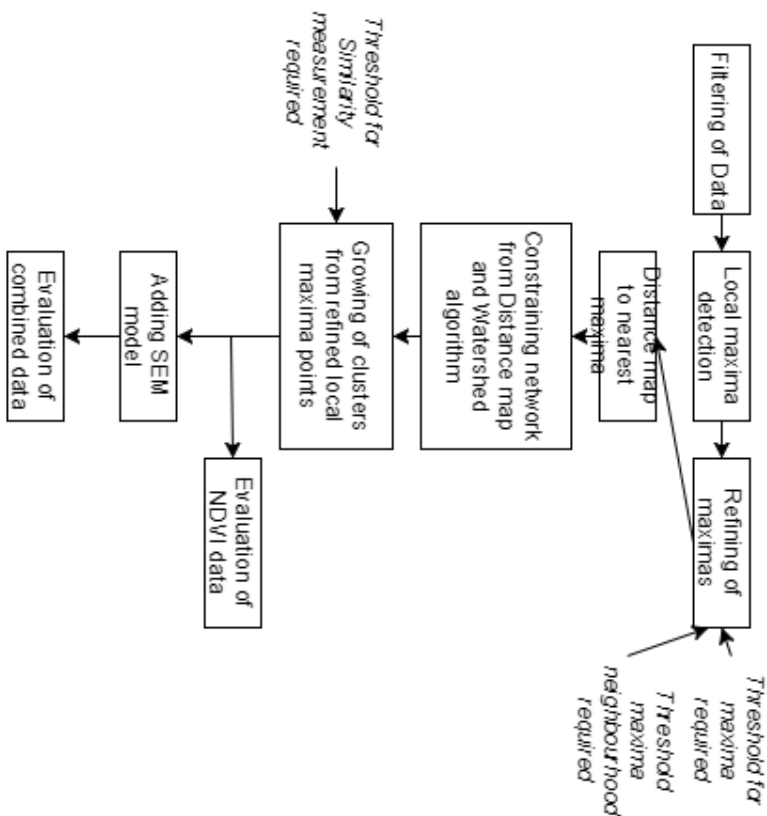


Figure 4.5: left: Original workflow, right: Adapted and optimised workflow for Matlab

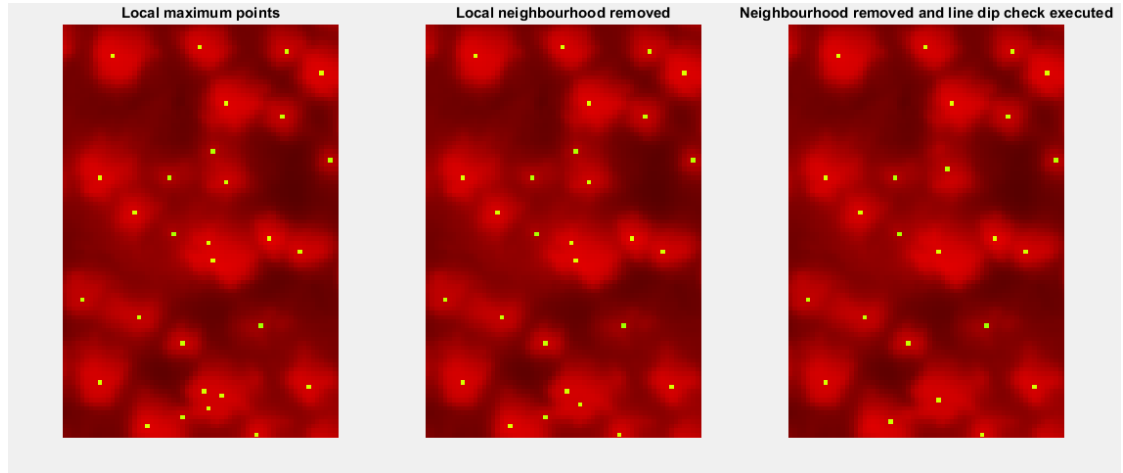


Figure 4.6: Improvement of maxima points

Instead of starting off with the raw data, the data is smoothed with a Gaussian filter with  $\sigma = 0.5$ . This removes small variation within the tree crown without affecting the tree boundaries too much. The local maxima are detected in a  $3 \times 3$  neighbourhood and are soft maxima ( $\geq$ ) instead of strict maxima ( $>$ ).

Since there will be local maxima in very shaded areas, a minimum intensity requirement for seed pixels is set as:

$$Min\_val = Threshold * mean(all\_seeds)$$

with *Threshold* being defined by the user in the range of [0-1].

Based upon a minimum tree diameter of 1 m and the assumption of a shaded area between trees, all maxima within a neighbourhood of  $7 \times 7$  pixels are joined and the resulting seed-point is adjusted based upon the removed maxima positions.

As a further refinement of the seed points and in inspiration by Culvanor's line checking, a line-check is conducted on all seeds that fall into a  $21 \times 21$  neighbourhood of a seed pixel. This check looks if there is a substantial dip

$$Sig\_dip = Threshold * center\_seed$$

between the seed points. If it can't find a dip between two or more points, the points are removed and a new point is calculated. Since this point is still required to be within the tree, a limit was implemented to limit the new points decrease in intensity

$$point\_min = mean(removed\_points) * ((1 + Threshold)/2)$$

If the intensity is not satisfied no points are removed. All these changes are to the maxima detection part of the algorithm.

Instead of basing the constraining network on the minima points (similar to Gougeon), I use a built in Matlab function to create a Distance map to the closest points, and run

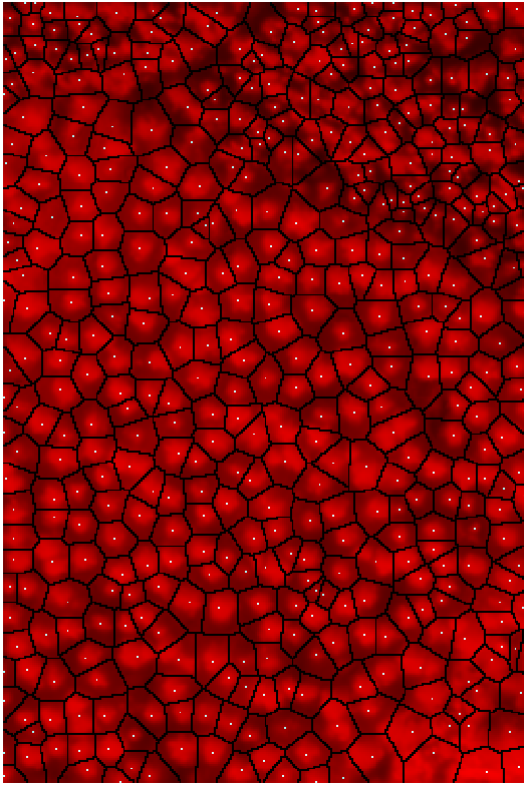


Figure 4.7: Constraining network and the maxima points it is based on

a built in Matlab function to create a watershed structure. This structure is a single pixel wide, contains one seed point per basin and can as such be used as a constraining network- (see figure 4.7). This results in a clearer separation between tree crowns, and reduces tree merging, which closed canopies are prone to when running the constraining network on the minima points. The use of the distant map does however connect foreground and background markers in a few cases, leading to a small underestimation in tree crowns.

Due to the Distance map/watershed combination, there is no possibility of multiple seed points within a single region, and as such the growing process does not need to be structured after the seed intensity.

#### 4.2.2 Addition of 3D information

Since the Region growing algorithm is based on seed points and a similarity measurement, the SEM model can be used directly, and requires only small alterations to the algorithm. The similarity measurement is changed from a pixel intensity similarity to a height similarity, requiring the pixels of the crown to be connected to the seed and no lower than 2 meters than the tree. The seedpoints are placed at SEM maxima, since the local maxima points should correspond to the tree tops.

### 4.3 Marker Controlled Watershed

Beucher and Lantuejoul introduced the idea of viewing the intensity of a gray scale image as elevation and then simulating run-off to create watershed regions in 1979 [5].

While the Watershed algorithm for separating image objects worked very well in theory, it falls short in reality. As Meyer *et al.*[32] observes in 1990 the real world situation is far from the theory since it includes noise and local minima, which all are surrounded with a divide line and thus leading to over segmentation. To remedy the over segmentation in the image, he works out a pre-classification for the image that restrains the waterflow dividing lines. The pre-classification divides the image into "spots" (objects of interest/foreground) and background. By applying these labels when running a watershed, dividing lines between the same classes are removed.

Wang *et al.* [52] further refined Meyer's general algorithm for forest applications. Due to the markers controlling the number of basins for the watershed, the marker selection has to be done carefully. Wang bases his marker selection a two way approach and fuses the collected information into a single set of markers.

#### 4.3.1 Creation of the tree object

The general tree-object is created from a single intensity band (in Wang [52] he uses the first PCA component) by applying a Laplacian of the Gaussian (LOG) detector stated as

$$LoG(x, y) = -\frac{1}{(\pi\sigma^4)} \left[ 1 - \frac{x^2 + y^2}{2\sigma^2} \right] \exp\left(-\frac{x^2 + y^2}{2\sigma^2}\right)$$

where  $\sigma$  determines the smoothing scale and the minimum edge width that can be captured. The original choice made in the article is  $\sigma = 1$  which corresponds to 1 pixel(60 cm) which is also the smallest crown diameter possible to detect. Phantom edges were removed and the result was used to create closed contours for each tree.

#### 4.3.2 Marker generation

With the objects from the LOG operator the treetop needs to be found. This is done by applying a local non-maximum suppression filter. Using a sliding window, the center pixels of the window is set to 1 if all the other pixel in the window are less than the centerpixel. The window size is an important factor. A large window might only detect one maximum in a case of joint trees, while a small window can detect multiple maxima due to within crown variations.

Since the tree object was created from the gradient image and outlined, it is a pure black and white image. Continuing on the assumption that the treetop is in the center of the tree at a nadir view angle, a geodesic distance transform based upon a 8 connectivity disk is executed. Once the distance between each pixel within the tree object to the border is found he uses a maxima approach to decide on treetops. The maxima approach is not based on single pixel value due to the trees not being perfectly round, so instead he defines the regional maxima as: "a connected group of pixels with a single distance

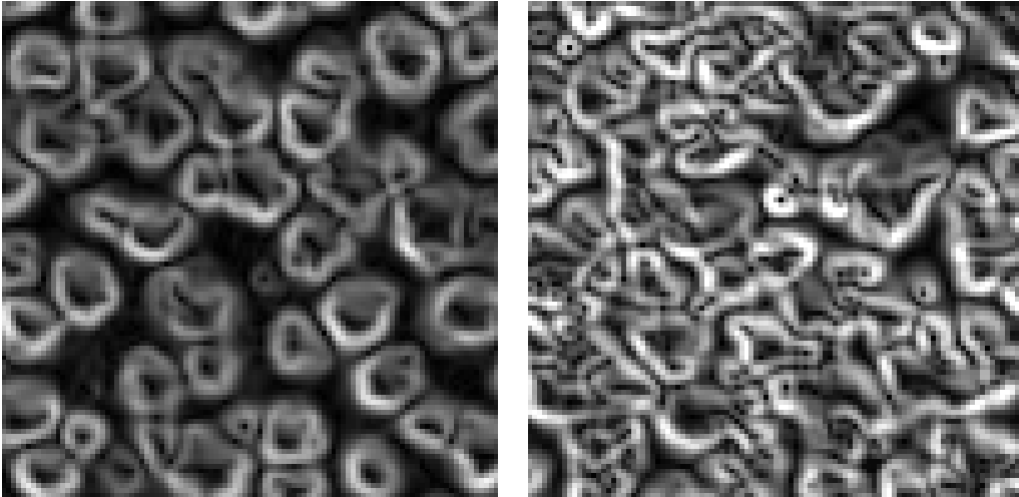


Figure 4.8: Gradient of illumination variation of closed forest cover. Left: Coniferous forest. Right: Mixed forest

value such that each pixel in the group has a value greater than or equal to all the pixel values within the surrounding eight-connectivity neighbourhood.” [52].

The markers found in the local non-maximum suppression filter are checked against the transformed distance markers, and if they are within a neighbourhood of 3x3 they are assumed to be correct, if not, they are removed.

### 4.3.3 Delineation of trees

The watershed in the algorithm is not run on the entire image at once as is usual, but it is rather applied to the tree objects outlined by the gradient image. The reason stated for this decision is that by cutting out the background entirely the noise and oversegmentation is reduced. The watershed algorithm does not run on the inverted part of the PCA one element as might be expected, but rather on another morphological distance transform which this time represents the distance to the closest marker for each pixel within the tree object. This distance transform is then used on the watershed algorithm to create boundaries between multiple markers within the same tree object. The dividing lines that are created within the tree object are then fused with the border of the tree object and are thus closed, delineated trees.

### 4.3.4 Adaption of original algorithm

Wang's algorithm is based upon his study area, which only included coniferous forest. He uses the predictable results from coniferous trees in an open canopy to create his tree objects. This solution does however not work on mixed or deciduous forest with a closed canopy. While the gradient is still a good indication of overall tree shapes, it is not possible to simply predict single trees in a mixed forest. (figure 4.8)

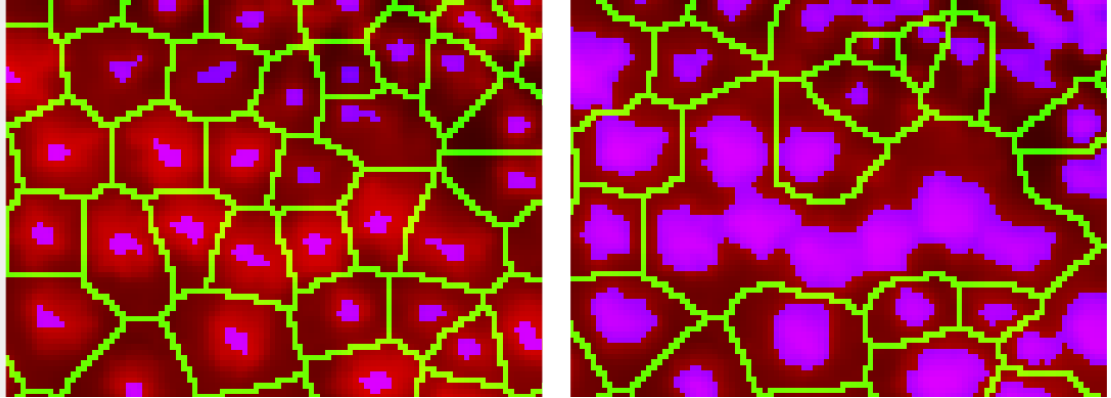


Figure 4.9: left: Watershed base on distance from treetop markers. Right: Watershed based on distance from Background markers.

Most of Wang's algorithm is based upon the tree object extraction from the edge detection which is impossible for parts of my forested area. As such I had to improvise while keeping to the same principles of marker controlled watershed.

My first goal is to create markers for the treetops. I apply an erosion and a reconstruction to the intensity band, flattening out the maxima. Running the same procedure on the inverse of the image produces smoother valleys. The structuring object for this is a 3x3 window with ones, giving eight connectivity and representing the smallest crown I want to detect. The markers are created by looking for the connected areas of maximum values that were created with the first erosion and reconstruction. The markers seem to fit well, and from here I have two possibilities to create background markers:

- Use an adaptive threshold to binarize the image creating background markers and create treetops based upon distance from the background markers
- Use a distance transform based upon distance from tree markers as background markers.

The difference between the results can be seen in figure 4.9. While the markers are not used directly, a distance transform from them is used in a watershed to define the final background markers. Since the background markers based on the actual background merge a lot of trees in closed canopy conditions, the background markers used hereafter are derived from the foreground markers. Once the background markers are set, I force the minimum of the gradient to be on both sets of the markers, resulting in an adapted gradient. The watershed is then run with the markers applied, resulting in one large drainage basin for all background markers, and smaller basins for the trees. These tree basins are the delineated trees.

## 5 Evaluon of tree delineation

Remark to the evaluation of the precision of the algorithms: Due to lacking in situ data, the evaluation has been done compared with a human interpretation of the image and its tree crowns. This means that the selection was made on visually, separable tree crowns, which might lead to a bias of the underestimation of merges, since the selected trees might be more distinguishable than the average tree. It was impossible to delineate the mixed and deciduous stands with certainty and the evaluation results are therefore split into a quantifiable section based upon coniferous trees and a more general evaluation of mixed and deciduous stands.

### 5.1 Valley following

#### 5.1.1 Blocking threshold

The selection of the intensity threshold is a significant factor in detecting less illuminated trees. With the sun angle being around  $35^\circ$  the possibility for a large tree to throw a shadow on a smaller tree behind it is significant in a dense forest canopy. *Figure 5.1* shows the result of an intensity threshold at 0.3 (which covers a total of 2% of the image), 0.4 (9% of the image) and 0.5 (33% of the image).

The thresholds behaviour was investigated on multiple images. While the best threshold to mask out canopy gaps was dependent on forest type, the percentage of pixels blocked was found to be around 10 % for closed canopy with limited canopy complexity. The 10 % estimation could make it possible to automate the threshold, removing the need for human input in the algorithm. However, this limits the application of

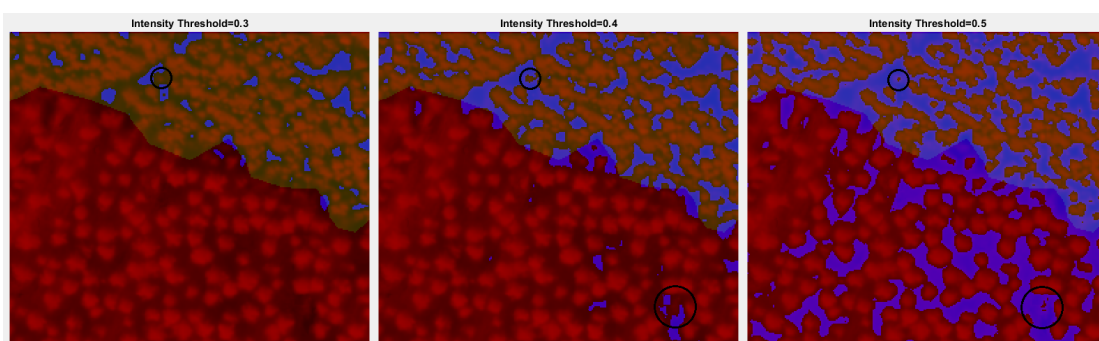


Figure 5.1: Showcase of losing trees to thresholding. Circled areas are disappearing trees. Orange tinted area is a mixed tree stand.

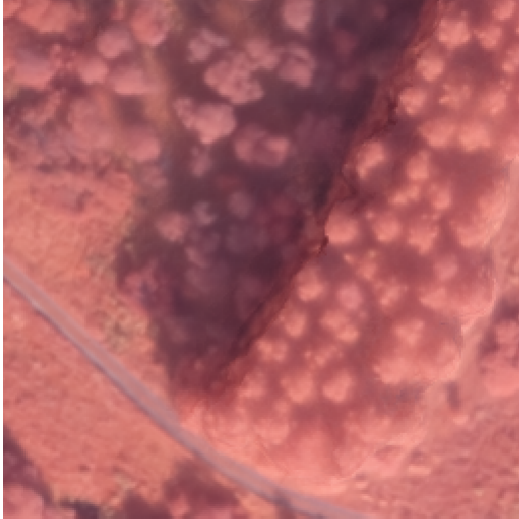


Figure 5.2: Large Poplar trees overshadowing their neighbours due to the low sun angle.

such an algorithm to pure forest canopy images, since an introduction of roads, fields or other biospheres change the reflectance distributions. In these cases, a large scale pre-segmented image would be necessary to eliminate non forested areas.

The height and canopy complexity are significant in the threshold, since the illumination angle is around  $35^\circ$  which results in a large shadow area. This shadow area can block out entire trees due to the reduction in illumination and thus reduce the observed radiance. In a complex canopy this happens to smaller trees while for large height differences between species this happens in the border regions.(figure 5.2).

While the self shadowing can be extrapolated to estimate biomass and diameter breast heights[25, 13] it is only of limited use in our algorithm in the creation of the valleys. This is due to the fact that most of the trees were planted simultaneously and have as such a limited height variation. It also creates a disturbance between tree species that has to be accounted for when delineation of larger images.

The height and canopy complexity influence on the results can be strongly reduced through a high angle illumination combined with a nadir view of a camera.

### 5.1.2 Valley following results

The results of the watershed algorithm with a Gaussian 3x3 filter with  $\sigma = 0.5$  can be seen in figure 5.3. The yellow tree crowns have been manually outlined under the principle that they represent the brightest part of the tree, and as such the delineation algorithm should show similar, if not a bigger tree crowns. Large amounts of marked tree crowns outside of the delineations are counted as underestimation. To reduce the human error element, a over/under estimation of 1 pixel for small trees and 2 pixels for large trees is permitted. Due to the way the algorithms rules are built, the algorithm can only split trees but not merge them. This means that any trees that should be merged

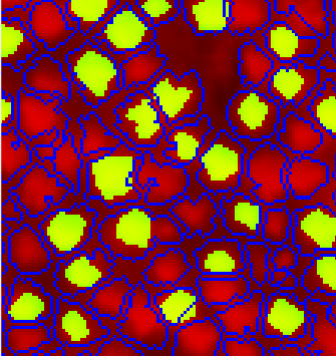


Figure 5.3: Delineation through Valley following. Yellow: Manual outlined trees. Blue: Automated boundary.

need to be merged through the pre-processing filter.

The results of the delineation results with different filters pre applied can be seen in table 5.1. The Valley following algorithm is clearly prone to overestimation and only manages to delineate 13 trees correctly as a maximum. The use of the filter does however show in the reduction of splits from one to zero, as well as in the slight reduction of overestimations. However, the increase in merges is a good argument against to much filtering.

Table 5.1: Valley following delineation results. G (Gaussian with alpha) A(Average with neighbourhood)

-	No filter	G 0.5	G 0.5 G 1	G0.5 G 1.5	G 0.5 A 7
<b>Correct</b>	9	10	13	12	9
<b>Underestimate</b>	0	0	0	0	0
<b>Overestimate</b>	87	86	82	83	70
<b>Split</b>	1	1	0	0	0
<b>Merge</b>	3	3	5	5	21

The mixed tree stand delineation behaves as follows:

Without any filtering, a large number of bright objects are circled well. The amount of splitted tree crowns is large and very large bright clusters are often not found or have only smaller extensions off them outlined. The in-crown variance throws of the algorithm from the larger trees, and combined with a maximum allowed tree boundary length of 250 pixels (75 meter or a mean radius of 11 meters) leads to merging and omissions of tree crowns. This results in the losses of the largest clusters.

When pre-processed with a Gaussian filter ( $3 \times 3$ ,  $\sigma = 0.5$ ) the mixed forest stand outlines are getting some of the larger clusters, while still omitting others.(figure 5.4,left) However, compared to without filtering, no cluster is completely omitted. There is still a lot of splitting within clusters and trees, and a lot of the smaller clusters are omitted.

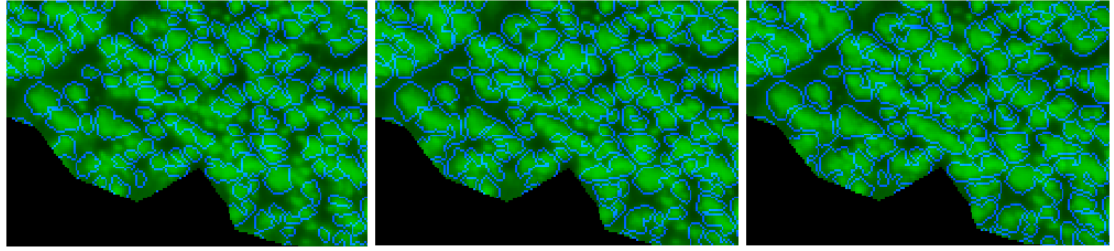


Figure 5.4: Delineation boundaries created by the Valley following with different filters. Left:Gaussian 3x3  $\sigma = 0.5$ . Middle:3x3 and 5x5,  $\sigma = 0.5$  and 1. Right:3x3 and 7x7,  $\sigma = 0.5$  and 1.5

Overall a slightly better fit that hits more trees than without filtering.

When run through two Gaussian filters (3x3 and 5x5,  $\sigma = 0.5$  and 1 respectively) filter the boundaries seem to fit very well, and almost all crown mass is enclosed in boundaries with the exception of a few smaller treetop or branches.(figure 5.4,middle) However, the merging of trees is becoming obvious, leading to chains of trees over 17 meter long. A lot of the merging might be correct but due to the nature of the imagery and lack of ground control, there is no way to tell with certainty if they are different trees or not. Over all it is a compromise between including more crown material in each crown, but also increasing the merging.

When run through two Gaussian filters (3x3 and 7x7,  $\sigma = 0.5$  and 1.5 respectively) the tree crown boundaries seem to find decent solutions most of the time.(figure 5.4,right) A few smaller trees are omitted, and a number of the smaller trees are merged with larger ones. There are some trees that create chains or cover a very large area but they seem a bit more natural here than with the 3x3 5x5 filter combination.

### 5.1.3 Application of SEM

The delineation with the Valley following algorithm based on the SEM model failed. Based on the few trees that it actually managed to find, were well clear of other trees. As such it is clear that the application of the Valley following model works only in an open canopy situation at the 25 cm resolution interpolated down from 50 cm resolution. There are two main error factors resulting in very poor delineation, the larger resolution and closed canopy. The closed canopy reduces the visual ground for UAV's and as such valleys between trees are not ground deep. Additionally a view-angle away from the nadir direction reduces the observable height differences.

## 5.2 Region Growth

### 5.2.1 Seed point generation

Due to the dependence of the algorithm on the tree detection through its seed points it is of interest to investigate the ways to obtain them, and their accuracy independent of

Table 5.2: Intensity for low intensity maxima removal and dip check threshold set to 0.75. All filters are Gaussian with the given  $\sigma$ . Each Check comes in addition to the previous checks

	Seeds/Tree	No filter	$\sigma = 0.5$	$\sigma = 0.5$ and 1	$\sigma = 0.5$ and 1.5
<b>Local Max</b>	0	0	0	0	0
	1	20	82	100	100
	>1	80	18	0	0
<b>+Neighbour Check</b>	0	1	0	0	0
	1	86	89	100	100
	>1	13	11	0	0
<b>+Dip Check</b>	0	13	8	12	11
	1	87	91	88	89
	>1	0	1	0	0

the delineation results.

The results of the seed point locations on coniferous trees gives clear indications on the behaviour of the seed point placement in coniferous forest. The threshold tables (*Table 5.2 5.3* show the results of the seed point placement in coniferous forest. The number of seeds located in each of the 100 manual delineated trees is counted and presented as either a correct classification (Seeds/Trees=1) or an over/under estimation (>1/0). The need for filter application is clear, since no threshold on its own manages to provide a single seed point per tree. While a small filter (Gaussian, 3x3,  $\sigma = 0.5$ ) increases the accuracy of the seed point placement, there is still a need to improve the results. Applying another filter of either medium (Gaussian, 5x5,  $\sigma = 1$ ) or large size (Gaussian, 7x7,  $\sigma = 1.5$ ), results in perfect seed point placement. It is clear that the coniferous trees are reliably distinguishable by combining two filters. There is no need for a more complicated check to see if the line between tree seed points actually crosses a valley. The filter sizes and  $\sigma$ 's were selected to be of no larger size than the treetops. A single Gaussian filter (5x5,  $\sigma = 1$ ) already provides a large reduction in maxima points, but is too small to cover the entire tree (covering a diameter of 125 cm), so it gives some trees with multiple maxima. This can be avoided by increasing the filter size and  $\sigma$  or by applying an additional smoothing filter beforehand. The application of an additional filter is favourable since it reduces the details less than a large-scale filter would and works within a tree crown with less reduction of the valleys.

The impact of the intensity dip change is, based on the results, not necessary for coniferous trees. Figure 5.5 shows that the changes done by the dip check are significant in the mixed forest stand. While it is reducing splitting, the resulting seed placement is far from ideal in some situation, and based on the fact that splits are preferred over merges, the seed points used hereafter will be based on the local maxima and neighbourhood check.

While the results are clear on that the threshold does not have a large impact on seed

5 Evaluation of tree delineation

Table 5.3: Intensity for low intensity maxima removal and dip check threshold set to 0.85. All filters are Gaussian with the given  $\sigma$ . Each Check comes in addition to the previous checks

	Seeds/Tree	No filter	$\sigma = 0.5$	$\sigma = 0.5$ and 1	$\sigma = 0.5$ and 1.5
<b>Local Max</b>	0	0	0	0	0
	1	20	82	100	100
	>1	80	18	0	0
<b>+Neighbour Check</b>	0	1	0	0	0
	1	86	89	100	100
	>1	13	11	0	0
<b>+Dip Check</b>	0	6	4	4	3
	1	93	96	96	97
	>1	1	0	0	0

Table 5.4: Intensity for low intensity maxima removal and dip check threshold set to 0.95. All filters are Gaussian with the given  $\sigma$ . Each Check comes in addition to the previous checks

	Seeds/Tree	No filter	$\sigma = 0.5$	$\sigma = 0.5$ and 1	$\sigma = 0.5$ and 1.5
<b>Local Max</b>	0	0	0	0	0
	1	20	82	100	100
	>1	80	18	0	0
<b>+Neighbour Check</b>	0	1	0	0	0
	1	86	89	100	100
	>1	13	11	0	0
<b>+Dip Check</b>	0	2	0	0	0
	1	96	99	100	100
	>1	2	1	0	0

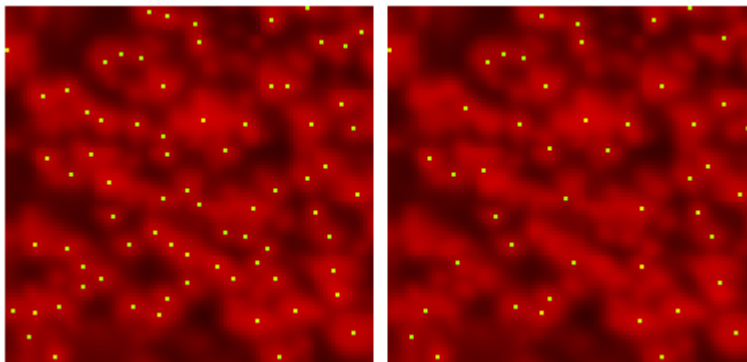


Figure 5.5: Seed points before and after the intensity dip check has been performed.

Table 5.5: Number of maxima points given for each filter set and maxima refinement methods. T = Threshold and all filters Gaussian with given sigma.

	Methode	T = 0.75	T = 0.85	T = 0.95
No filter	Max	1609	1444	1309
	Neighbour	811	432	644
	Dip	439	482	547
$\sigma = 0.5$	Max	832	763	657
	Neighbour	736	677	587
	Dip	426	472	515
$\sigma = 0.5, 1$	Max	608	556	455
	Neighbour	595	545	450
	Dip	367	413	416
$\sigma = 0.5, 1.5$	Max	524	482	381
	Neighbour	517	475	378
	Dip	358	383	357

points for coniferous trees if filters are applied, the numbers of maxima found still varies within the image based on the thresholds (Table 5.5). This change in number of tree seeds is based in two areas, the Pinus mungo with their irregular shapes and the grass land in the image. While the changes in the grass can be neglected due to it not being of any interest for our application, the changes in the Pine stand need to be evaluated.

Figure 5.6 show a clear depiction of what is happening when raising the minimum threshold for the seed points intensity. The losses are low reflectance trees and branches, probably shadowed by neighbours. Figure 5.5 (right) reminds of the height shadow effect depicted earlier in figure 5.2 and since the area is a change in forest stands it is likely that this is the reason for the large amount of shadowed trees. Based on the images the threshold of 0.85 is chosen as it reduces the amount on seed points outside of trees in the coniferous stand, and the overall loss within a mixed tree stand is small when discounting boundary areas.

### 5.2.2 Growth delineation results

With the seed points found, the only factor left to consider in the region growing algorithm is the similarity measurement which is used to determine if a pixel belongs to the crown pixel or not. A surprising find was that it does not matter what version of the image is used in the cluster growing process. Once the seed points are established the growth results based on a filtered image, with the same filters as where used to find the seed, and the unfiltered image are precisely the same. This is an interesting result for larger images, since it makes it possible to do all operations on a single image, without the need to pass along the original image as variable, thus freeing up memory resources.

The results of the delineation are show in table 5.6. It shows the similarity measure-

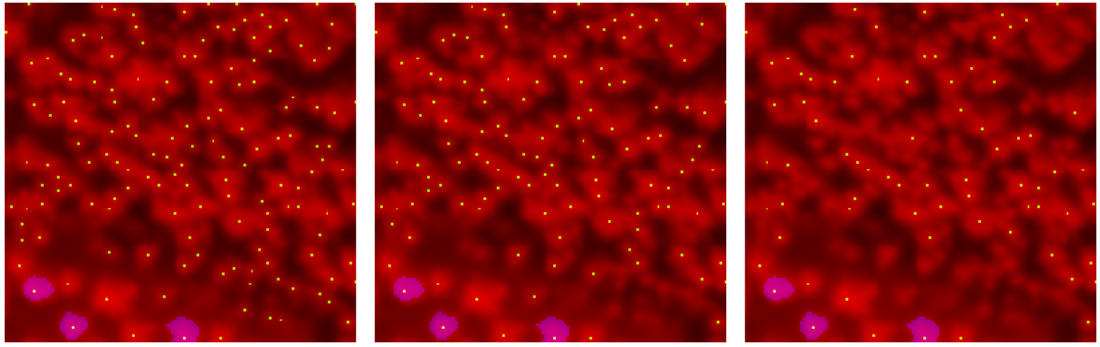


Figure 5.6: Seed points after the neighbourhood check for thresholds of 0.75 0.85 and 0.95 respectively.

Table 5.6: Cluster growing with different similarity thresholds.

	T=0.65	T=0.75	T=0.85	T=0.95
Correct	46	88	53	0
Underestimate	1	8	47	100
Overestimate	53	4	0	0
Split	0	0	0	0
Merge	0	0	0	0

ment threshold of 0.75 is resulting in the most correctly outlined trees. As the similarity thresholds increases, the underestimation increases as well (lower part of the images in figure 5.7). This can be used in spectral measurements since it focuses on the brightest part of the tree crown, and at a height similarity threshold it is quite certain that all points that belong within the automated outline belong to the tree crown.

The same trends of increasingly underestimating the tree crown is true for the mixed forest stand. The number of splits is large due to the many seed points in the stand and as such none of the outlines can be used as true trees. But the outlined results can still be used, since they do encircle brighter spots that could be tree crowns or large branches. This leads to multiple measurements per tree. When comparing the delineation for the different similarity thresholds only the 0.65 threshold seems to include larger amounts of non-tree crown material. The 0.75 does a good job at outlining the clusters, and shows only a limited intensity variation within an outline. The 0.95 similarity threshold gives only the minimal tops, with some only being the seed itself. The 0.85 threshold does include a bit more crown material than the 0.95 threshold but still underestimates the trees significantly. As such the best outline threshold is 0.75 for a mixed forest stand. Since both evaluations concluded with the 0.75 similarity threshold showing the best results it means that a pre-segmentation is not necessary.

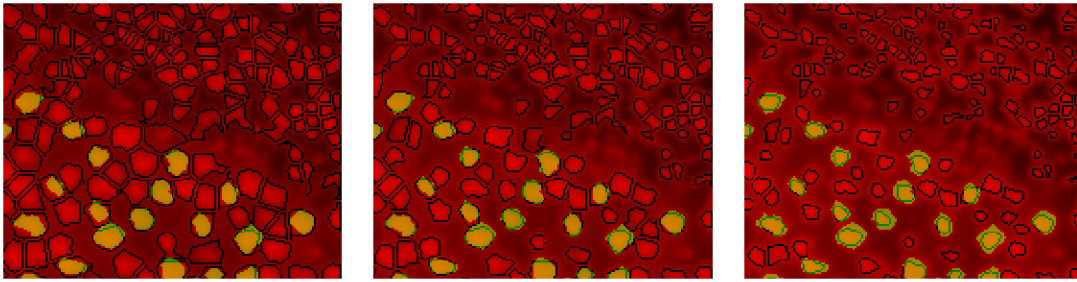


Figure 5.7: Region growing with similarity thresholds at 0.65,0.75 and 0.85 respectively. Upper part of the images is a mixed forest stand, lower part is a coniferous stand. Yellow spots represent manually outline tree crown material.

### 5.2.3 Application of SEM

The SEM model approached showed that while the concept is valid, the accuracy at 50 cm resolution is its downfall. Out from the 100 manual outlined trees, 44 were without seeds. The large amount of tree loss can not be contributed to the interpolation. In fact, a bicubic interpolation increases the number of maxima points, but still underestimates greatly. The evaluation of the SEM model for use in combination with the NDVI camera was stopped at this point, since it was clear that the large amount of tree losses and the placement of the seed points would not be able to improve the NDVI region growing results.

## 5.3 Marker controlled watershed

The marker controlled watershed provides two data sets of interest. One is of course the delineation of the tree crown, while the other is the foreground markers. The foreground markers serve the purpose of the tree detection and can as such be used to extract very small tree crowns from them.

Due to the nature of the geomorphological functions, an unfiltered image results in larger foreground markers than when applying filters. The markers in a mixed forest stand are not the best fitting markers to begin with, and additional filtering removes and shrinks the markers, which leads to a larger omission of trees. However, the markers seem to not have any problems with varying intensity throughout the image since no direct thresholds are implemented. This means that border areas of stands and stands with high amounts of shadows are still marked quite well. Applying filters to images reduces the accuracy and number of markers in mixed forest stands.

The coniferous stand results ( table 5.7) show that a applying filters does improve the detection and delineation results. The delineation results are the most precise result compared to the manual outline in comparison with the other algorithms. However, the complete loss of three trees is a heavy argument against the algorithm. Since complete losses of trees should be avoided, filters must be applied. This implies that a pre-

Table 5.7: Marker controlled watershed results with filters

	No filter	$\sigma = 0.5$	$\sigma = 0.5 \text{ and } 1$	$\sigma = 0.5 \text{ and } 1.5$
Correct	90	91	96	94
Underestimate	0	0	0	0
Overestimate	7	7	4	5
Omission	3	2	0	0

segmentation into forest stands is necessary to achieve the best results.

When running the same algorithm on the first PCA element, the omissions are reduced by one while the underestimate increases by one. This improvement is offset by more omissions in the mixed forest stand.

## 5.4 Conclusion on Tree delineation and Spectral application

The application of UAV's is still in an early state with new approaches and instruments being developed frequently. The publications about tree delineation based on passive optical UAV data is limited. The publications concerning SfM for closed forest canopies even more so. While SfM applications have proven viable for plantations [36] and open canopy situations. Our results show clearly that optical delineation algorithms are not obsolete, or entirely replaceable by three dimensional data. The delineation algorithms adopted from high resolution optical satellite imagery satellite optical data works on mosaicked UAV data . The higher resolution increases the amount of information in each tree crown which requires filters to be applied. While the application of filters is working as intended, it was found that an averaging filter should be avoided if possible, since a gaussian (a circular filter) catches tree crowns far better while distorting intensity differences less. The application of different filters and their influence on the end results was also investigated, since it is a step regularly neglected in published literature. Our results show that I kept tree seeds for our coniferous trees in a somewhat open canopy even when applying large gaussian filters. Suggesting that coniferous trees in a somewhat open canopy are resilient against over filtering as long as the filters are of circular nature. An irregular, closed canopy was providing better results when applying larger filters due to the higher amount of in crown variance. However, filter application on irregular, closed canopy forest for classification purposes has to be investigated further with concern to tree delineation. The question of splits and omissions is something that needs to be carefully evaluated in an objective way and based on ground truth, both of which were not done here as such ground truth was not available.

Our results for CHM models showed that the approaches were not viable. The reason for the results is a combination of factors. Based on the resolution alone, our approaches where rather crude since our applications, designed for sub 50 cm resolution, would be looking for larger tree crowns. While the SfM algorithm has been shown to work, the application of a structured grid, compared with data points ( figure 5.8) results in averages, reducing details. This means that tree crowns can be flattened, and tree

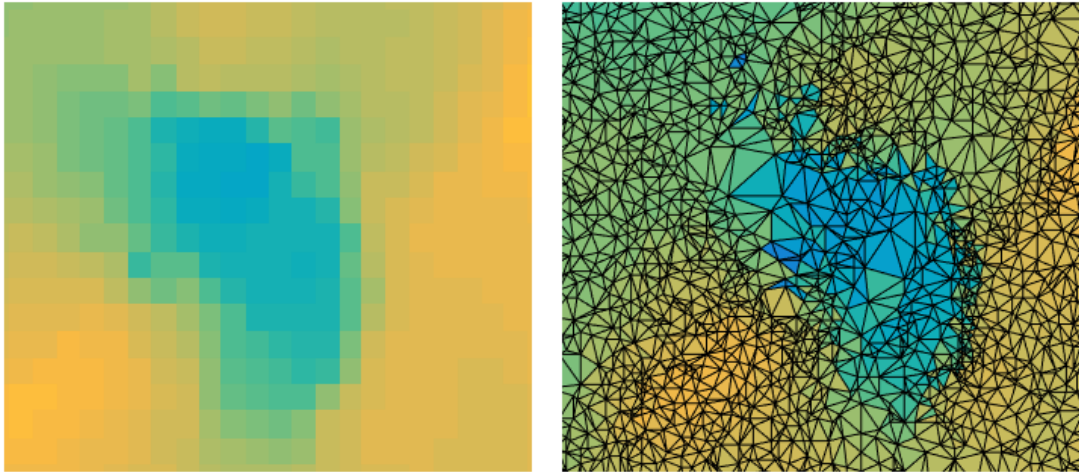


Figure 5.8: Left: Averaged SEM 0.5 meter resolution. Right: Original SfM point cloud.

tops suppressed in the end results, which also explains the  $\sim 50\%$  reduction in found treetops. While CHM models are frequently used in tree delineation and classification, as it provides valuable height and texture data, the SEM model in itself was found to be of little applicational value in our case due to the lack of a DEM model.

Going forward in the tree delineation the focus will most likely be on passive optical delineation for high resolution imagery (25-50cm) and photogrammetry on the very high resolution (5-15cm) data. The resolutions of passive imagery and SfM point clouds can be easily increased by different mission planning, leading to lower flight heights or by using higher quality cameras. The use of 3D point clouds for delineation is already wide spread for very high resolution applications, and will likely continue. Passive optical tree delineation, even though an older topic, is still under development for applicational use on satellite imagery.

The approach to hybrid CHM models, based upon a lower resolution DEM model paired with a photogrammetric SEM model, is already being investigated, and with the steadily increasing amount of LIDAR based DEM models available might prove a good, low cost approach to offset the main negative traits of the photogrammetry problems.

The need for a generalized evaluation system for tree delineation is clear, and while some work has been done toward this direction, it only encompasses the older, more general delineation methods. I recommend that a general evaluation procedure gets established on a fixed dataset containing first and second LIDAR returns (canopy and ground) at high resolution, photogrammetry point clouds, as well as IRGB and CIR high resolution imagery. These sites would need to cover a large range of species and climates to create a common comparison possibility. Further a clear set of evaluation rules of what is considered a correct tree outline would need to be established as well. It is important to stress the importance to unify the evaluation methods, since many small algorithm changes have been done, but cannot readily be compared to any existing work. While application specific evaluations certainly have their place (as is the case

## 5 Evaluation of tree delineation

for our results) a generalized approach will provide significant improvements and time savings when considering algorithms to investigate.

For my spectral investigation I want to, ideally delineate every tree since invasive species detection is one of the possible application to a delineated dataset. Thus i set three guidelines for the evaluation of the delineation:

- Avoid omissions
- Splits are better than merges
- Reduce overestimation

### 5.4.1 Evaluation for spectral application

#### Valley following

The results of the Valley following (*Table 5.1*) means that the best pre-processing for our case of coniferous trees is the single Gaussian filter with  $\sigma = 0.5$ . While not giving the most correct trees, it does give less merges than any other filter (except without filtering) and since the trees are to be analysed individually, a favour of splits over merges is preferred. The Valley following algorithm constantly overestimates the tree crowns (compared with the manual delineation). This is a factor that has to be accounted for when using the tree crown in spectral analysis, since shadowed leafs have a non linear modified reflection profile [11] compared with the sunlit reflection profile. For the irregular shapes of the pine stand the amount of trees split is very large as is the complete omission of crown material. This means that the double Gaussian filter  $\sigma = 0.5$  and  $\sigma = 1$  is fitting since it includes more crown mass. This also means that for spectral evaluations, the image need to be segmented into leaf types before processing.

#### Region Growing

The region growing delineation looks promising for the extraction of spectral data. The ability to influence the strictness of the within tree crown makes it a versatile algorithm to compare the results to the other algorithms. A threshold of 0.65 which overestimates the tree crown boundaries can be compared directly to the Valley following algorithm, while a stricter boundary of 0.85 can be directly compared to the markers found by the marker controlled watershed. The ability to segment a variation of trees, without previous pre-segmentation makes it more versatile and the same results on filtered and unfiltered imagery makes it memory efficient at a larger scale. Another good argument for the algorithm is that due to the selection of seed points the grow constrained merged trees are impossible. There were some slight overlaps between manual outlined tree crowns and two different region grow outlines, but those where within the tolerance set to compensate human error.

### **Marker controlled Watershed**

The marker controlled watershed algorithm provides the best tree outlines for coniferous forest. The drawback is that a pre-segmentation of forest stands is necessary. In a mixed forest stand the algorithm performs rather poorly, outlining only a few trees. In the borders between stands, the algorithm shows a better result than the other algorithms. Overall the algorithm is the best performing algorithm for a coniferous forest stand with filters applied. When using the results for spectral measurements, the markers might be used to create a baseline for comparison to other measurements due to their focus on the tree crowns.

### **Conclusion**

The following spectral investigation will be mainly based upon the Region Growing algorithm due to its selectable crown size. The different crown sizes can be used to investigate the non linear shadow variations as well as providing a strict definition to counteract mosaicking errors.



## 6 Methods and implementation of spectral investigation

High spatial resolution of the spectral data provides a lot of details. The application of such high resolution data needs to be considered carefully, since it might increase processing time for applications that are shown to work for lower spatial resolution. Tree species classification has been shown to work at 1.5 meter scale [10] and for land cover classification resolutions are even larger [55]. As such, it is of interest to show that a targeted reduction in the data sets can reduce the processing time as well as improve the classification results.

### 6.1 Use of Rikola Spectral data for delineation

All delineation so far has been done on the modified consumer Canon Powershot camera. However, the infrared observation capabilities are present in both cameras on the flight, and since the delineation algorithms presented are executed on a single band intensity, the application of the delineation algorithm should work on one or the sum of more bands that cover the infrared range in the Rikola camera as well. The infrared bandwidth of the Powershot camera is approximately  $720 \text{ nm} \pm 50 \text{ nm}$ . Table 3.3 shows there are 3 channels in the same range for the Rikola camera. For the application evaluation of the Rikola imagery to the delineation phase, each band, as well as the sum of all bands is linearly rescaled to the range of [0-1] for the delineation algorithm.

### 6.2 NDVI

The normalized difference vegetation index (NDVI) is defined by formula 6.1 where Near infra red (NIR) and the red channel (RED) correspond to the surface reflectance of their respective bands. The NDVI is used to investigate the possibility for live green plants in multispectral imaging, due to their characteristics of absorbing the RED bands, while reflecting NIR bands. The large difference in the reflectance and absorption behaviour can be used to investigate images to see if they contain the typical chlorophyll reflectance patterns. Since the NDVI is built upon the reflectance pattern of chlorophyll, the index is quite sensitive to changes in the chlorophyll, and since the amount and of chlorophyll is dependent on the plants health, and the environment around it, the NDVI is sensitive to the conditions of the areas the plant lives in. Stresses applied to the vegetation changes the amount and behaviour of the chlorophyll and thus the reflectance. These stress factors can then be indirectly observed through the chlorophylls reflectance behaviour.

## 6 Methods and implementation of spectral investigation

One of these stress factors is the accessibility of water and the relationship to the NDVI has been used in drought monitoring[43]. Näsi *et al.* [40] used the NDVI together with spectral measurements to map Bark Beetle Damage on trees. While he investigates the possibilities to map the damage on a tree basis he concludes that an average of the brightest datapoints from each tree crown achieves the best classification results. He argues that by using the average of the brightest part of the tree he reduces the deviations for the classifications, and that this process is reliable since Bark Beetle damage affects the entire crown, and only rarely single branches, thus being reflected in the few tree crown pixels used.

As such, a factor that Näsi does not use, and that tree delineation opens up for analysis, is the variation within a single crown. The standard deviation of the NDVI index should be able to discern onset of stress factors much earlier than a traditional pixel based spectral analysis since the standard deviation in a single tree should be small and comparable with the standard deviations of surrounding trees from the same species. The use however, is limited to stand segmented images, since a comparison needs to be made, and healthy values need to be established. It stands to argue that while he points out that the Bark Beetle damage mostly affects the entire tree crown, there is no certainty that the within crown variation will not change in comparison to healthy trees. While I do not have access to the data and ground truth, and as such can only make a guess at the actual application effect, I can investigate the standard deviation behaviour of the NDVI index within a single tree crown. While the data used in this study was not intended for an investigation of the affects of stress factors and therefore no ground truth towards this intent was collected, I might still be able to show a reduction of the standard deviation within the tree crowns.

To show that the reduction in standard variation is actually a result of the tree delineation, and not just the  $\frac{1}{\sqrt{N}}$  reduction coming from the standard deviation formula 6.2, a comparison against a block average with the same number of samples is made. This provides a comparison baseline to see if the tree crown standard deviation behaves differently from the stand standard deviation. Further, with the flexibility in the tree delineation algorithm used, the crown boundaries can be selected to tune the trees to specific size.

The calculation of the NDVI is stated in equation 6.1. For the data available, multiple channels cover the spectral ranges of RED and Infrared. The channel 7 at 706.15 nm and channel 15 at 866.69 nm have been chosen as RED and Infrared respectively, since both are lying central in their regions.

$$NDVI = \frac{NIR - RED}{NIR + RED} \quad (6.1)$$

$$s_x = \sqrt{\frac{\sum_{i=1}^n (x_i - \bar{x})^2}{n - 1}} \quad (6.2)$$

### 6.3 Automated classification

Support Vector Machines (SVM) are a type of algorithm introduced to pattern recognition in the mid 90's [49]. It is based on the assumption that two different classes can be separated by a hyperplane. This means it is possible to find a vector  $\underline{w}$  that defines a hyperplane and a bias  $b$  such that the classes can be optimally separated with the greatest margins. In an ideal case, with separation between the classes, the discriminant function  $f(\underline{x})$  deciding between the memberships takes the form:

$$f(\underline{x}) = \underline{w} \cdot \underline{x} + b \quad (6.3)$$

where  $\underline{x}_i$  is the point to be classified. When expanding the ideal concept to a more realistic situation with slightly mixed classes, and expanding the linear SVM to a non-linear SVM by using higher dimensions we end up with a discriminant function:

$$f(\underline{x}) = \sum_{i \in S} \alpha_i y_i K(\underline{x}_i, \underline{x}) + b \quad (6.4)$$

where  $\alpha_i$  are the non zero Lagrange multiplier, and  $K(\underline{x}_i, \underline{x})$  is the Kernel function. The optimization of the cost function then becomes:

$$\begin{cases} \text{maximize} : \sum_{i=1}^N \alpha_i - \frac{1}{2} \sum_{i=1}^N \sum_{j=1}^N \alpha_i \alpha_j y_i y_j K(\underline{x}_i, \underline{x}_j) \\ \text{subject to} : \sum_{i=1}^N \alpha_i y_i = 0 \text{ and } 0 \leq \alpha_i \leq C, i = 1, 2, \dots, N \end{cases} \quad (6.5)$$

For a more detail I refer to Melgani and Bruzzone [31] who explain how to arrive at these results, as well as the application to hyperspectral data.

The SVM deals efficiently with large spatial variability of the spectral signatures for the classes and have been proven to provide reliable classification for a range of forest application including some very high dimensional classifications[9].

A significant downside to the SVM is its binary nature. There are multiple approaches of how to implement a multi-class support vector machine. The most common implementation is the one-against-all(OAA) strategy[31]. The OAA approach works by creating an individual SVM for each class and a datapoint is processed by all SVMs. A discriminant function value is used to find the winner of the classification approach, and the winner classifies the datapoint.

Since the SVM is supervised, it requires labelled samples to be trained. This means that a classified result of the SVM is labelled according to the users specifications. For the dataset in this thesis, there is a total of 15 spectral bands available. While more spectral features could be computed (such as the NDVI, means...), a decision against it was made due to time and computing hardware constraints. The addition of spectral features would also have reduced the spectral improvements through tree delineation. All classification run for this thesis were implemented in Matlab and make use of the function *fitcecoc* provided in the MATLAB Statistics and Machine Learning Toolbox[30] with the OAA approach and empirical prior probabilities.

The training data was created by using the single species tree stands. This was done since spectral measurements from open source spectral libraries are collected under different circumstances. Their measurements are often taken on ground with spectroradiometers, providing a high spectral resolution. Deviations from the ground measured spectrum compared to the aerial spectrum are introduced due to influencing factors such as atmospheric distortions, camera calibrations, incident and reflection angles which change scattering behaviours.

## 6.4 Classification performance

The evaluation of the performance of the multivariate SVM's is done by looking at both general performance and species specific performance. Two measurements for the overall accuracy are used in evaluating the results, the overall accuracy (equation 6.6) and, due to non uniform training samples, Cohen's kappa. Cohens kappa (equation 6.7) measures the agreement between two observers, and takes into account the possibility of random agreement based on the number of samples classified. By setting one of the observers to correspond to the training data, and thus the truth, a direct comparison can be made.

$$\text{Observed accuracy} = \frac{\text{Correctly Classifications}}{\text{Numer of Samples}} \quad (6.6)$$

$$\text{Kappa} = \frac{\text{Observed accuracy} - \text{Expected acuraccy}}{1 - \text{Expected acuraccy}} \quad (6.7)$$

$$\text{Expected accuracy} = \frac{1}{N^2} \sum_{i=1}^K c_i * t_i \quad (6.8)$$

where  $K$  is the number of separable classes,  $c_i$  is the number of samples classified to belong in class  $i$ , and  $t_i$  is the number of samples in the truth of class  $i$  and  $N$  is to total number of samples.

On the class basis both Recall (i.e. User Accuracy, equation 6.9) and Precision (i.e. Producer Accuracy, equation 6.10) are given, showing the performance for each class classification.

$$\text{Recall} = \frac{\text{tp}}{\text{tp} + \text{fn}} \quad (6.9)$$

where tp is the number of positive classifications that are actually positive (True positive) and fn is the number of negative classifications that are actually positive (False negative).

$$\text{Precision} = \frac{\text{tp}}{\text{tp} + \text{fp}} \quad (6.10)$$

where fp is the number of samples classified positive that are actually negative (False positive).

While the tree delineation does reduce the amount of datapoints used in the classification process, making it possible to use the entire data set instead of a subset, the

calculation capacity due to the repeated creation process of the multivariate SVM required to perform a leave-on-out(LOO) classification scheme could not be met. A ten fold cross validation was implemented as a compromise between classification accuracy and computational requirements. This means that the results created from evaluations are not accurately reproducible, due to a random segmentation of the data. However, these should only result in small variation on the overall statistics.

### 6.5 Species information in the standard deviation

The Standard deviation of tree crowns(formular 6.2) has been mentioned in the contexts of the NDVI and its possibilities to add value to the tree stress classifications. Another interesting and as far as I found, unpublished question is the possibility to use the standard deviation of the spectral values of the tree crowns in the classification process as an additional source of information. Computing additional features for tree species classification is nothing new, and used in LIDAR data in the form of Energy, Correlation, Homogeneity and Contrast[14]. For hyperspectral data features such as Minima values and mean spectra and normalized mean spectra have been used[38], though only to a limited extend. This means that a classification attempt purely based on the standard deviation of the tree species will be done to see if the standard deviation alone carries any species information.



## 7 Results of spectral investigation

### 7.1 Rikola data for delineation

The Rikola bands within the same infrared range as Canon Powershot were evaluated separately as well as summed together and normalized. The result for each band, as well as the combined result of the bands is shown in figure 7.1. Every red crown in the images is a crown delineated by the modified Canon IR band, but not by the IR band from the Rikola camera. While it shows that the IR bands from the Rikola camera can be used for delineation purposes, it also shows that the omission rate is clearly higher than for the Canon Powershot.

When taking a close look at the delineation results an offset between the Rikola and Canon camera can be seen in the northern direction (figure 7.2). The variance and differences between the sensors led to an adjustment of the similarity measurement for the Rikola camera, as it was found to produce the most similar tree crown to the Canon delineation (similarity =0.85) when the similarity of 0.6 was used.

### 7.2 Comparing spectral library values with measurements

The spectral reflectance profiles for **Picea glauca** and **Larix sibirica** were acquired from the open access spectral library SPECCHIO [18] and were in turn contributed to the library by Hovi *et al.* [17]. The reflectance profiles were normalized by using the largest reflectance value found in each spectrum, resulting in infrared tail after the red edge being zero. A blockaverage of the high resolution data was used to create the lower resolution comparison values. All spectra based on the Rikola data have been normalized by the same method as the library spectra so that the shapes of the spectral reflections can be compared. The normalization aids in the classification of features, and their proportions. All pixels that were used in the comparison were, when possible, manually picked from inside a tree crown. The results can be seen in figure 7.3.

Some features from the acquired ground measured spectrum can be identified in the UAV's measurements, but seem offset and/or strongly reduced. While the measurements used for figure 7.3 were manually selected point measurements from treetops, the situation is not better when looking at all pixel spectra in a single tree crown. There are large spectral deviations in a single tree crown, even though the similarity required to the seed (thick black line) was within 15 % of the infrared value of the CIR image (figure 7.5).

While some features from the acquired ground measured spectrum can be identified, the divergence is deemed too large to use for evaluations and automatic classification,

7 Results of spectral investigation

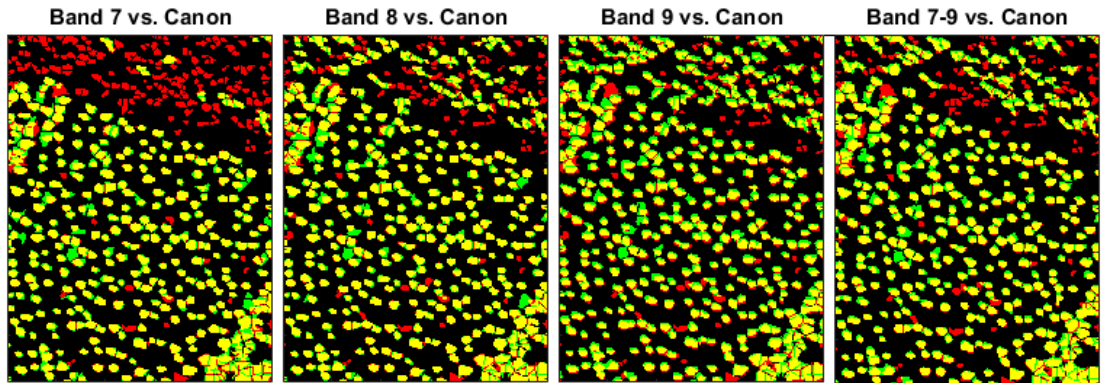


Figure 7.1: The delineation results for each band compared the Canon delineation. Red are tree crowns from Canon, Green are tree crowns from the Rikola bands. Overlap is yellow.

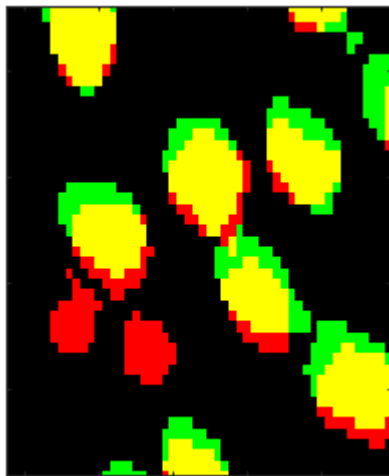


Figure 7.2: A clear offset between the two delineation results in the northern direction. Red are tree crowns from Canon, Green are tree crowns from the Rikola bands. Overlap is yellow.

## 7.2 Comparing spectral library values with measurements

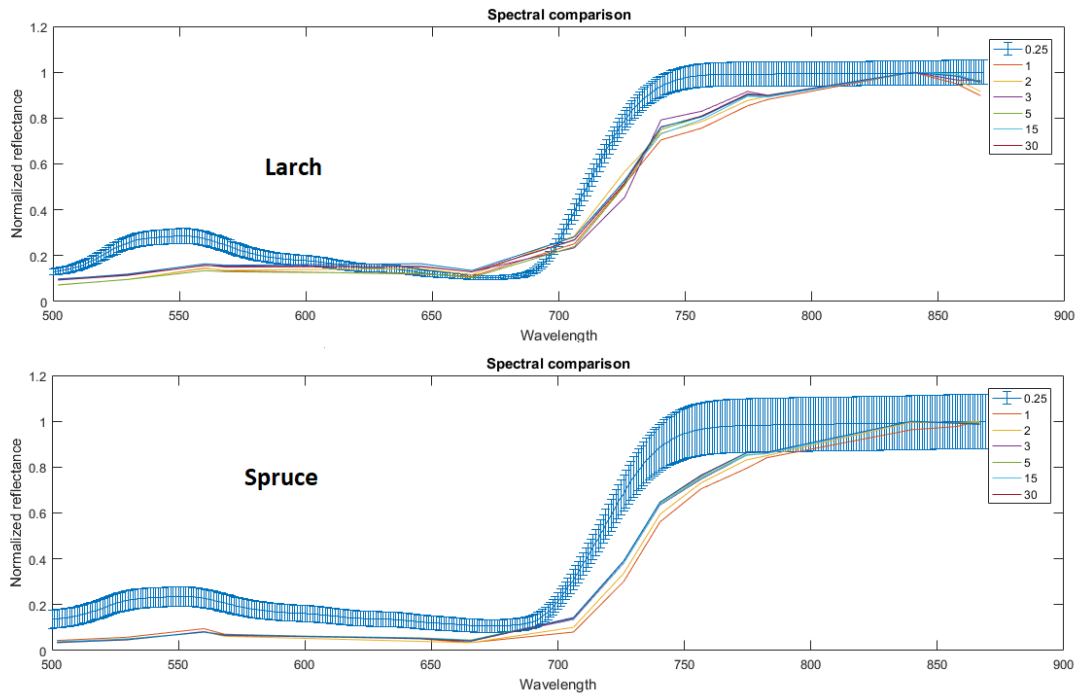


Figure 7.3: Background error bar plots are showing the spectral values from SPECCHIO for the corresponding species. Each spectra line corresponds to the scaled resolution given in the legend in meters.

## 7 Results of spectral investigation

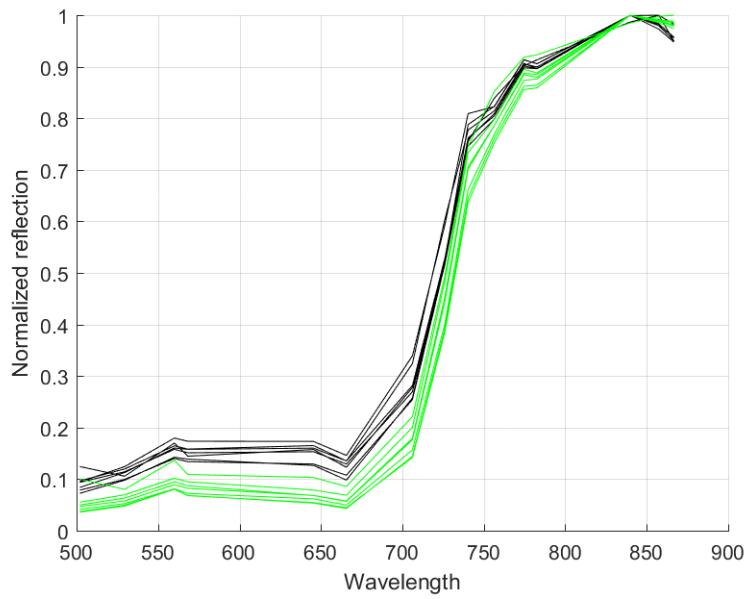


Figure 7.4: Showing the normalized reflection for Spruce(green) and Larch(black) for multiple sizes of tree crowns.

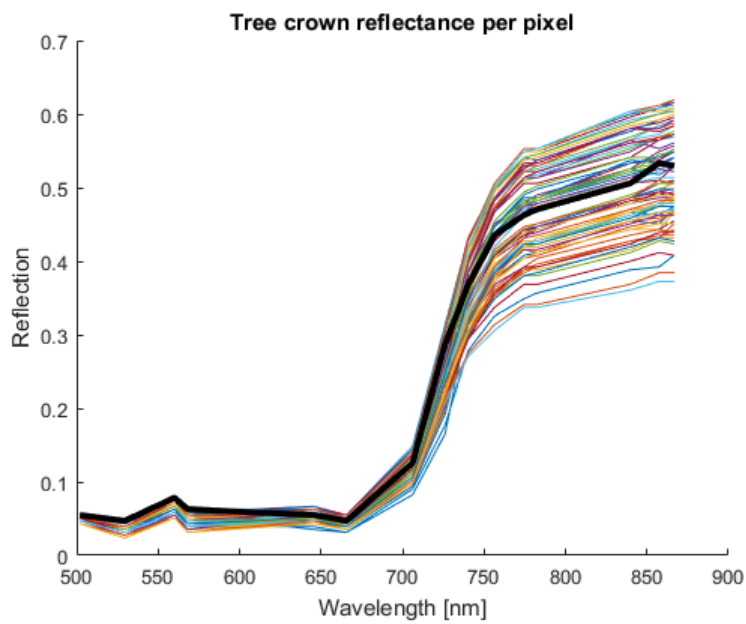


Figure 7.5: Spectrum plotted for each pixel identified to belong to the same tree crown. Seed is the thick black line.

### 7.3 NDVI standard deviation improvement

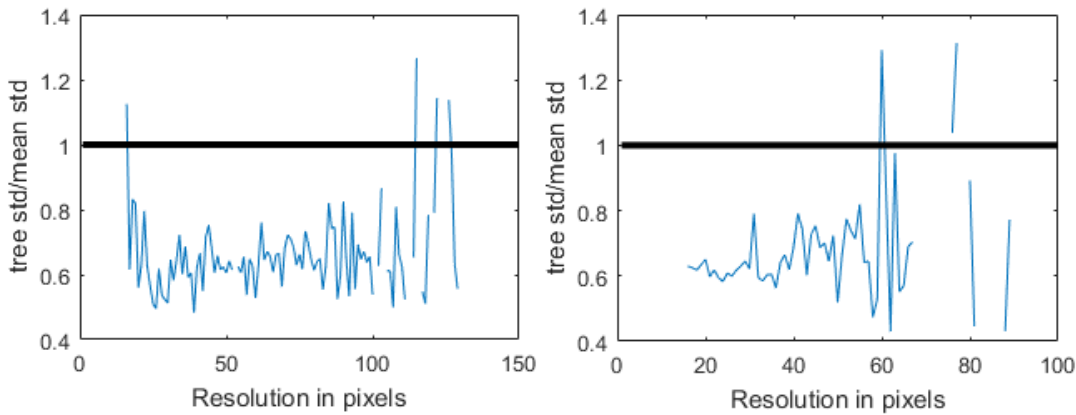


Figure 7.6: The Ratio of the standard deviation of the single trees compared to the same resolution of the entire stand image. Below one is an improvement. left: Larch. right: Spruce.

and will therefore be left out in the following work. It is worth noting however, that a classification between the species is possible, as can be seen in figure 7.4 where the normalized reflectance spectra of Spruce and Larch are plotted together. While some wavelengths in the normalized spectra match, as is expected, since both spectra are normalized, it is clear that the lower reflection in the lower bands, as well as the onset of the red-edge are features that can be used to separate the species.

### 7.3 NDVI standard deviation improvement

The NDVI was calculated from channel 7 and 15 from the Rikola camera (706.15 nm and 866.69 nm respectively). The NDVI was calculated for a range of resolutions, which were created by degrading the original Rikola image data through a block average. The standard deviation for the NDVI was calculated across the image for each resolution, creating a comparison baseline which accounted for the sample size in the average and removed the  $1/\sqrt{N}$  connected to the sample size, thus providing a baseline to be compared to the NDVI standard deviation of the single trees.

Compared to the standard deviation of the entire NDVI image, as would be present for a sensor with a lower resolution, the delineated trees show a standard deviation reduction of up to 60 % as can be seen in figure 7.6 for most trees. Both sets do have outliers with standard deviations far above the clustered results but they are few and mostly contained in the largest tree crowns. While the standard deviation of the entire image continues to reduce with increasing resolution, due to the increased number of samples within each average, an average of around 1000 pixels or a resolution of 7 meters, is necessary to reach the same standard deviation as the delineated tree crowns, where the largest crowns are around 300 pixels in size.

## 7.4 Automated classifier results

The automated classifier was created using the function `fitcecoc` in the MATLAB Statistics and Machine Learning Toolbox[30]. This function creates the SVM's needed to classify the data. In addition to the Data and Labels, the function accepts more specification. In my case, I did not use the default classification algorithm of "one Vs. one", but "one vs. all" since it reduces the amount of binary learners for the classification from 10 to 5, thus reducing the computational time, since less SVMs need to be trained. The effect of the computational time reduction is directly proportional with the binary learners, and in my case results in a 50% faster algorithm as well as a slightly faster classification since every point to be classified only requires 5 evaluations and not 10. While the increase in computational demand is linear with the amount of classes for the "one vs. all" due to the amount of learners being  $K$  with  $K$  as the number of classes, the "one vs. one" with the amount of learner given by  $K(K-1)/2$  is close to quadratic. The prior probabilities were set to empirical, since the training datasets were not properly balanced. The use of parallel computation was also enabled to increase the speed of the calculations.

All resulting SVMs classifier were evaluated against the training datasets, since these datasets were the only available ground truth. The largest dataset contained 487 438 datapoints which would have made a leave one out cross validation (LOOCV) scheme a time consuming affair. Thus I opted for a tenfold cross validation instead. While a LOOCV would have been possible for the mean tree value datapoints, I went with tenfold cross validation instead to be consistent over all datasets. The ten fold cross validation separates the data into 10 segments randomly, leading to slight variations within the results. This means that these results are not reproducible down to the single point scale, but the overall accuracy were within 0.1%.

Table 7.1 shows the result when using all pixels(487 438 datapoints in total) belonging to the pure forest stands. These pixels include shaded areas and even ground pixels visible tree gaps. With an overall accuracy of 72% the classification is far worse than any recent published literature. The classification algorithm seems to have large problems in the classification of Silver Spruce and Norway Spruce. Especially the separation between those two classes seem to a point of contention, resulting in Recall and precision values around 0.5. meaning that their classification is almost a random selections, with slight biases towards the truth due to wrong classifications to or from other species. Another interesting value is the recall value for Larch at 0.9833, which is an exemplary classification rate considered against the results of far larger studies encompassing more identifiers.

The processing time of the entire dataset took approximately one hour and 35 minutes, running on a 6 core 3.3 GHz processor. Due to the "one vs. all" classification method used, only 5 workers (and as such only 5 cores) were used since only 5 separate classes were present and only 5 SVMs needed to be calculated at the same time. This means that a scaling to 6 separate species is trivial and should not influence the computational time as long as the amount of datapoints remains the same.

Table 7.2 shows the classification results using all datapoints determined to be within

Table 7.1: All pixels within the pure treestands

Overall accuracy=72.0%		Classified as					Recall
Kappa=0.6345		Birch	Larch	Pine	Silver Spruce	NorwaySpruce	
<b>True Class</b>	Birch	72057	1832	902	12300	10666	0.7371
	Larch	1294	152770	6	778	518	0.9833
	Pine	206	8	22906	6844	2124	0.7138
	Silver Spruce	9967	4071	3890	54287	31967	0.5211
	Norway Spruce	9142	2055	2945	34937	48966	0.4994
<b>Precision</b>		0.7776	0.9504	0.7474	0.4974	0.5196	

Table 7.2: All pixels classified to be in tree crowns of the delineated pure stands

Overall accuracy=80.3%		Classified as					Recall
Kappa=0.7413		Birch	Larch	Pine	Silver Spruce	Norway Spruce	
<b>True Class</b>	Birch	31610	657	25	1385	2095	0.8837
	Larch	567	44385	3	249	85	0.9800
	Pine	17	2	8380	1190	169	0.8588
	Silver Spruce	2526	1071	1087	18142	4357	0.6674
	Norway Spruce	2807	598	447	8358	10553	0.4636
<b>Precision</b>		0.8423	0.9502	0.8429	0.6187	0.6114	

a tree crown with the tree crown delineation done by the region growing algorithm under the same parameters as where determined to be the best for our application (Chapter 5). The amount of datapoints is reduced by 70% to 146 093 points. The evaluation of the classifier was again done with a ten fold cross validation, resulting in minute changes in the result due to the random selection of the ten groups of data. The evaluation was done against the points classified to belong to a tree and not every pixel within the true forest stand, since the goal is to classify the trees, and not the ground around the trees. From the results we can see an improvement in the overall accuracy of 8.3%. On a class bases Birch, Pine and Silver Spruce show varying improvements in all Precision and Recall values in the range of 0.07 to 0.14. Larch does decrease slightly in both recall and precision, 0.0033 and 0.0002 respectively, while Norway Spruce Recall reduces by 0.036 and precision increases with 0.1. The processing time on the same system as described earlier was approximately 22 minutes, a 75% reduction in computational time. The delineation algorithm's processing time was a couple of seconds for each pure tree stand and comes in addition to that.

Table 7.3 shows the classification results for the mean spectral values of the trees.

## 7 Results of spectral investigation

Table 7.3: The mean values calculated for each delineated tree in the pure stands selected

Overall accuracy=81.6%		Classified as					Recall
Kappa=0.7649		Birch	Larch	Pine	Silver Spruce	Norway Spruce	
<b>True Class</b>	Birch	764	6	0	29	37	0.9139
	Larch	9	767	0	10	4	0.9709
	Pine	0	0	351	25	5	0.9213
	Silver Spruce	37	20	14	792	196	0.7479
	Norway Spruce	45	7	4	274	527	0.6149
<b>Precision</b>		0.8936	0.9587	0.9512	0.7009	0.6853	

Each tree crown that is detected by the delineation algorithm is labelled separately, and all spectral values of each labelled area is than averaged. These average values are than used in the training of the classifier, as well as in the ten fold cross validation to evaluate the results. A total of 3923 trees were found and resulted in the same number of datapoints to be used. While the overall accuracy did only increase by 1.3% the performance of the classifier in terms of Recall and Precision did increase with 0.03 to 0.09 for all values expect for the Recall of Larch, which reduced by 0.01. This results in accuracy above 95% for Larch and Pine 89% for Birch and the Spruce classes at 69% and 68% respectively. The computational time required was approximately 130 seconds, to which the delineation phase and averaging of tree tops need to be added with about 3-4 seconds per tree stand.

The results of an actual classification are shown in figure 7.7 where the sample area 1 is classified with the tree crowns spectral averages. It can be seen in the top part that the classification mixes Norway Spruce and Silver Spruce in the top of the image. This is in truth **Pinus mungo** for which i did not have any training data. The consistent Larch classification on the lower part of the image corresponds with the ground truth. The lower right corner is an open grass area and not of any interest for our tree classification purpose.

### 7.5 Spectral Standard deviation

When evaluating the standard deviation in all bands, and not only on the NDVI, the same trends are visible. The standard deviation for tree crowns is mostly below the standard deviation for the entire image at that resolution. (Figure 7.8). While the majority of trees is well below the standard deviation of the image at an equivalent averaged number of pixels, trends are visible. Larger crowns tend to have a larger standard deviation in the spectral measurements , even under strict similarity measurements when delineation the tree crowns. It is however worth pointing out that the values for tree crowns with more than 50 pixels are point measurements of single trees, since the number of large

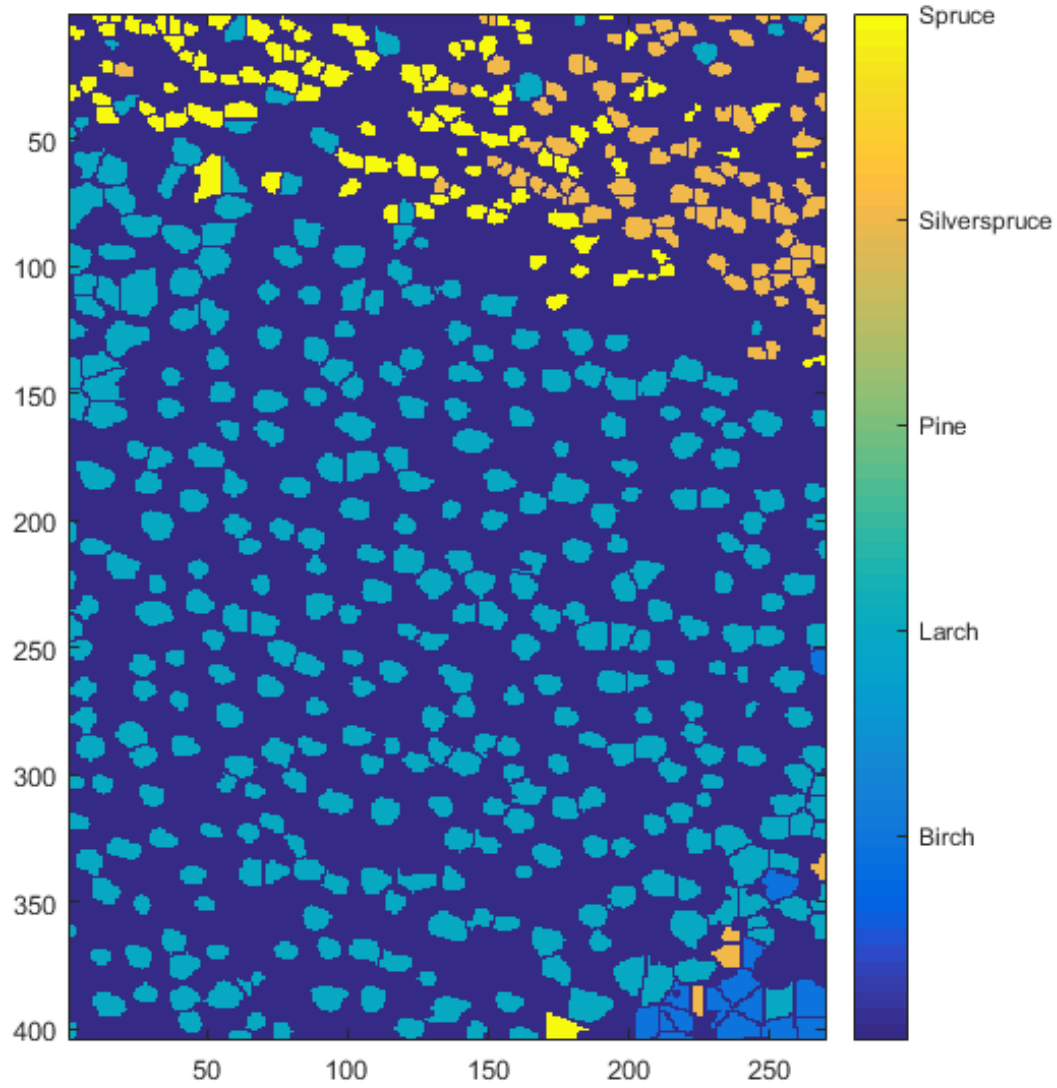


Figure 7.7: The classification results based on the SVM classifier trained on the tree crown averages.

## 7 Results of spectral investigation

Table 7.4: The classification result based on the standard deviation

Overall accuracy=62.5%		Classified as					Recall
Kappa=0.5186		Birch	Larch	Pine	Silver Spruce	Norway Spruce	
<b>True Class</b>	Birch	556	165	2	80	33	0.6651
	Larch	70	547	7	110	56	0.6924
	Pine	9	10	186	102	74	0.4882
	Silver Spruce	17	88	47	758	149	0.7158
	Norway Spruce	44	69	65	273	406	0.4737
<b>Precision</b>		0.7989	0.6223	0.6059	0.5729	0.5655	

trees was limited within the samples.

### 7.6 Species information in the standard deviation

Since individual crowns have been established, the standard deviation for each collected band of each tree crown can be calculated. This results in 15 standard deviation values for each tree crown corresponding to the 15 collected Rikola bands. These spectral features were used to train a SVM classifier to see if the standard deviation contained any species information. The result of the 10 fold cross validation can be seen in table 7.4. A kappa of 0.5186 shows that the classification results are not in correspondence with a random distribution. An overall accuracy of 62.5% was achieved. The worst performing class was the Pine, seeing more than half of the trees misclassified, while the Silver Spruce was split less between its self and Spruce as seen in earlier spectral classifications.

Since the standard deviation values in my dataset do contain species information it is of interest to see if the information is an addition to the spectral classification or simply a surplus which is already contained in the spectral values. Since the standard deviation only works at tree level, the mean tree spectral values are used. These combinations result in 30 variables for each tree, and the classification results can be seen in table 7.5. Compared to the mean tree spectral values (table 7.3) the overall accuracy increases with 1.7% while the Kappa only increases with 0.0211. The confusion matrix tells us that the addition of the standard deviation information increases the Recall of Pine Silver Spruce and Norway Spruce, reducing in particular the mix between Norway Spruce and Silver Spruce. For larch the Recall is almost unchanged (increase of 0.013) while Birch is actually losing accuracy (reduction of 0.012).

## 7.6 Species information in the standard deviation

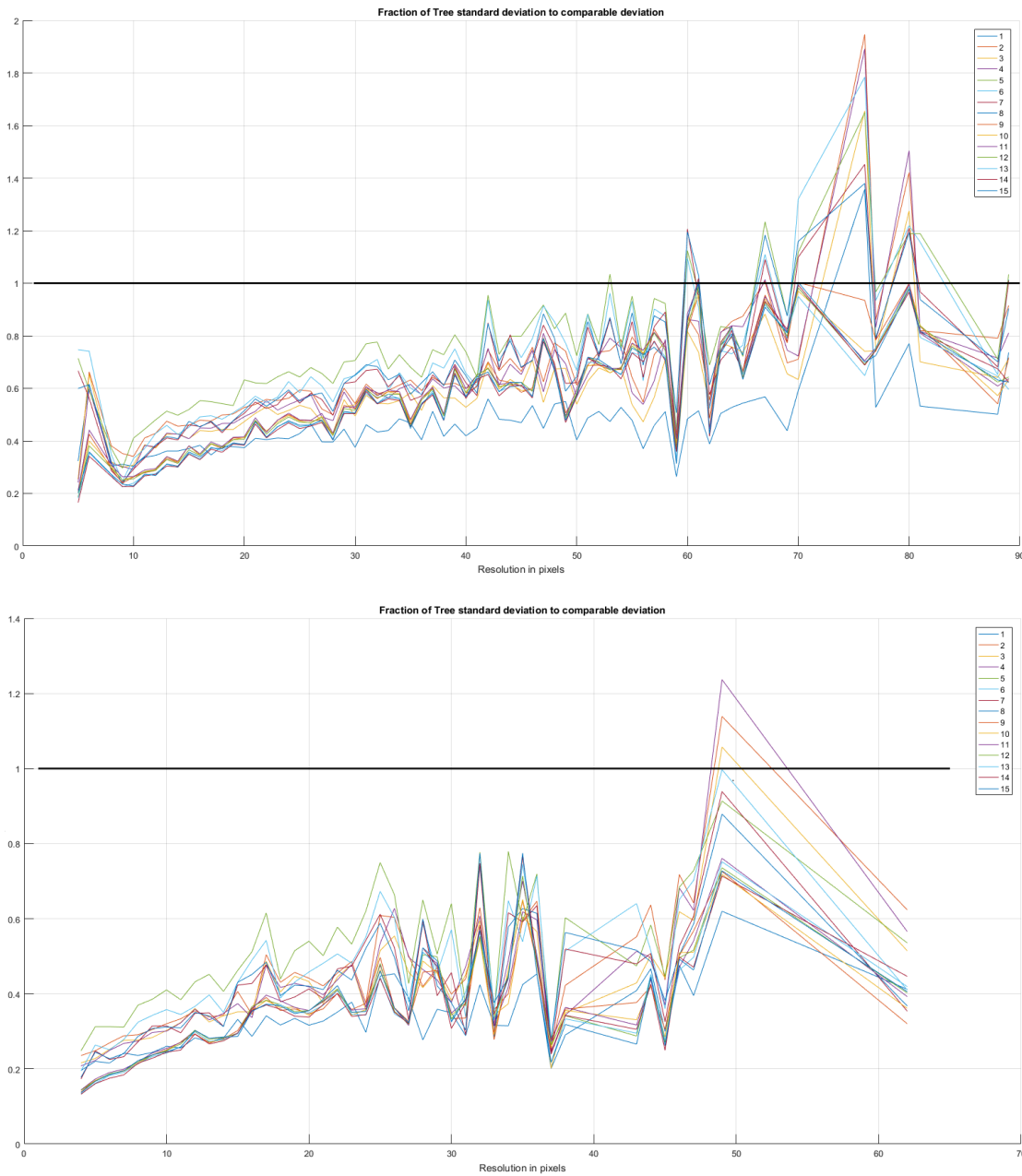


Figure 7.8: The Ratio of the standard deviation of single trees compared to the same resolution of the entire stand image. Each line represents a Rikola band. Below 1 is an improvement. Top: Similarity measurement of 15%, resulting in well delineated tree crowns. Bottom: Similarity measurement of 5%, resulting in underestimated delineated tree crowns.

7 Results of spectral investigation

Table 7.5: The classification result on the mean tree spectral values and the standard deviation

Overall accuracy=83.3%		Classified as					Recal
Kappa=0.7860		Birch	Larch	Pine	Silver Spruce	Norway Spruce	
<b>True Class</b>	Birch	754	5	0	36	41	0.9019
	Larch	6	768	0	8	8	0.9722
	Pine	3	0	359	16	3	0.9423
	Silver Spruce	35	17	16	836	155	0.7894
	Norway Spruce	41	5	3	259	549	0.6406
<b>Precision</b>		0.8987	0.9660	0.9497	0.7238	0.7262	

## 8 Discussion

### 8.1 Rikola data for delineation

From the results of the comparison between the delineation results (figure 7.1) combined with the offset (figure 7.2) some sources of errors can be identified. The obvious offset between the NDVI image delineation result and the Rikola delineation result is a product of two different factors. The first is the high resolution nature of the data combined with the slight offset between the cameras as well as shutter speeds. While the area was extracted using a geo located mask, the resulting images from the mask, while having the same resolution, had a slight offset to each other. This resulted in some Rikola/NDVI sets having a size difference off one pixel in each direction. This was solved by removing the last column and/or row as necessary to match the image sizes. While not ideal, a complete image resize to a new grid would have resulted in an averaging effect over the image, based on the resizing method. For the NDVI camera this would have been fine, since smoothing was applied anyway, but I wanted to look at the raw data to see the effects of filtering, so I opted against a general resize. I would like to point out that the resize and offset do not influence the delineation result, since the offset was done prior to manual outlining tree crown. The offset effect became first visible when directly comparing delineation results between the two cameras. The second factor is the nature of the Rikola band collection. Since the 15 bands are collected individually, they are all offset from each other. In the coregistration and mosaicking the bands were coregistered into groups, and then mosaicked. Those groups then got coregistered to each other. This means that the coregistration between these groups can be off. One of these group splits was between 8 and 9, which can lead to an offset in the images to each other, resulting in an offset compared to the Canon image. Another interesting behaviour is that a reduction in the similarity measurement is needed to extend the tree crowns to similar dimensions than the Cannon camera. A smaller collection bandwidth creates less differences between the high reflectance tree crowns and the background and shaded area. As a consequence of this reduction in similarity measurement, some tree crowns extend into shaded areas leading to merging of tree crowns. Overall it can be established that a payload of two cameras is beneficial for the dataset. The increased amount of observed energy due to a larger bandwidth is beneficial to the delineation. In the figure 7.1 the partly correct classification of Larch (lower part of Sample 1) can be seen. A further refinement of optical delineation algorithms can bring the Rikola delineation up to the same precision as the Canon Powershot, which in turn reduces the necessary payload of the UAV.

## 8.2 The use of spectral libraries

It is clear from figure 7.3 that the SPECCHIO values do not align with the UAV collected measurements. The most obvious feature mismatch is the location of the red-edge, which seems to be approximately 20 -25 nm delayed behind the ground truth. There are a couple of error sources possible.

- The instrument used for the ground truth was a ASD Field Spec 4 Standard-Res which operates with a larger number of bands, and far smaller bandwidth than the Rikola camera in a laboratory environment and executed on single leaves or collection of needles. This means that the wavelength ranges that are used to evaluate the reflection are more localised. While a more precise measurement are useful, an integration of the Field Spec bands corresponding to the collection area of a Rikola band does not result in the same values due to the sensor sensitivity not being equal to one across all wavelengths.
- Errors introduced by the atmospheric correction of the Rikola imagery visible as negative reflectance values. The Rikola sensor was calibrated before flight with a target approximately 1 meter away from the camera. Due to a flight height at 300 meters, Rayleigh scattering of the lower bands that were collected needs to be accounted for, which was not done in this dataset. This results in a suppression of the blue bands (as can be seen in figure 7.3).
- Errors introduced through the mosaicking of Rikola imagery. The mosaicking of the images creates image overlap and there are different solutions to merge the images, ranging from averaging across multiple overlapping images to using only nadir parts of images and cutting any overlapping parts. An average could change spectral values if a misalignment or optical distortions are present.
- Non lambertian reflection from leaves, combined with a multi angle combination through mosaicking. A lambertian reflectance is an idealization, which does not hold for forested areas on either leaf or tree scale. As such, an illumination angle of 35° will lead to different reflectance observations, both within a single image and across images.

Due to at least some of these influences, the reflectance patterns from the UAV does no correspond to the in situ measurements. it does however validate that there are structural differences in the spectra that can be used to separate the tree species, as long as a training data set is based on the Rikola data and not on the in situ measurements.

## 8.3 NDVI standard deviation

The reduction in the NDVI's standard deviation was working as expected for the averaging and in compliance with the results shown by Matese *et al.* [29]. Further, a reduction of the standard deviation was expected for  $\frac{1}{\sqrt{N}}$  as

minimum was expected, the standard deviation of a the single tree crowns where large. While this can be expected due to the elimination of shaded areas and ground areas, the impact was large compared with the values for the closed canopies. I can not show that the standard deviation of the NDVI can predict recently onset stress factors since my dataset was not collected with that purpose in mind. However i was able to show that there is a large reduction in the standard deviation for individual tree crown. And while some stress factors, such as Bark beetles might influence the entire crown [40], it is not clear weather these kind of stress factors are effecting the spectral response uniformly enough to keep the standard deviation of the entire crown, across all spectral bands the same. For stress factors affecting parts of the tree crowns, or spreading from a single start point of a tree crown, the standard deviation on a tree crown basis might prove to be a valuable feature. The evaluation of the NDVI standard deviation was done combining both the Rikola data and the Canon Powershot data. The Canon Powershot data was used for the delineation while the Rikola data was used to create the NDVI. I suggest that the influence of stress factors on the standard deviation can be investigated by using a CIR camera instead of the combination of multiple sensors, reducing payload requirements as well as co registration and mosaicking work. A CIR camera could also eliminate any offset between datasets due to geo location.

## 8.4 Classification results

### Complete Pure stands

The use of the entire spectral tree stands gives the worst delineation results of spectral classification with only an overall accuracy of 72%. (table 7.1). This does not come as a surprise, as large amount of shaded areas and even ground values observed between tree crowns are used in the training of the classification algorithm. Some tree species such as Larch as clearly easier to delineate than others. The worst offenders of misclassification are Norway Spruce and Silver Spruce. This mix is not surprising. The species are in the same family, and a close look at the mean spectral values figure 8.1 quickly establishes that the major difference in the species reflectance are the overall scaling of the reflectance values. By multiplying the spectral values of Sivlerspruce by a factor of 1.5 the reflectance spectra show large similarities. It is worth noting that the spectral reflectance values shown in figure 8.1 should be within the range of 0 to 100, while this is true for Silver Spruce, it is not for Norway Spruce. This an error introduced through the calibration process on ground, at a distance of 1 meter ,while the flight height of 300 meters was used to acquire the data. Some deviation from the maximal value of 100 has to be assumed to be present, since light irradiation might have increased during the one hour flight time of the UAV, and thus leading to larger observations of reflectance than physical possible. This similarity of spectral values when scaled to each other might be the reason of the large amount of classification between the species, since Matlab's SVMs normalize the training input data, which leads to only minute differences in the spectral values.

The overall classification with an accuracy of 72 % and a Kappa of 0.6345 is low

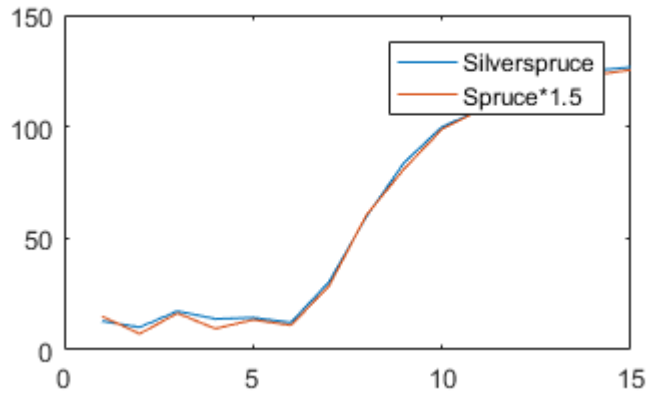


Figure 8.1: The reflectance values for Norway Spruce and Silver Spruce, where the Norway Spruce values are multiplied by a constant of 1.5

compared to other studies that use the SVM classifier [10], which receive only similar low results with a Gaussian maximum likelihood classifier. However, a 72% accuracy is quite good when comparing the number of features used for classification where I only used 15, compared to Dalponte *et al.*'s [10] 52 to 290.

### Tree crown pixels only

The delineation of the tree crowns based on the Canon Powershot Infrared channel removes most of the datapoints that are not contained within a tree crowns. This means that the training data provided for the classification algorithm is more concentrated and can provide better separation between the species, since common elements, such as ground pixels are not present in all classes. This is however, not entirely true, since an offset between the delineation result and Rikola data has already been established, though the reduction in background points removed is still significant, removing a total of 70% of the datapoints from the pure tree stands. The results seen in table 7.2 and show an improvement in the classification accuracy by 8.3% and an improvement of Kappa by 0.11. The reduction of the data to only contain tree crowns is an effective strategy, even without an average of the spectral values. Silver Spruce and Norway Spruce are still the major contribution for the wrongful classifications, while the other species can compete with the results of far more encompassing datasets[38].

### Mean tree values

The mean tree values provide an interesting dilemma. The results can be seen in table 7.3 and show an overall accuracy improvement of 1.3%. This alone is a nice improvement, but the averaging reduces the sample size from 146 093 points to a mere 3923 points. While the data reduction improves computational time massively, it also introduces more variation in the results. The dataset contained approximately 700 trees of each species, and as the sample size grows smaller, the resulting SVM classifier becomes less precise

due to the lack of training data. At a tenfold cross validation, almost 400 trees are removed from the training data, which is a significant amount when an entire stand only contains 700 trees. This makes the result of the tree classification based on the averages more volatile, and in turn increases the overall accuracy from 0.1 to 0.3%. If this approach to tree delineation purely based on the tree average spectral values is developed further, a strong emphasis need to be based on the sample size of each pure tree stand. In addition the trees should be evaluated with a LOOCV approach, and not with a ten fold cross validation. Instead, the use of the spectral mean values might instead be used as additional information, similar to what Nevalainen *et al.* [38] did where the mean values from a few selected bands were added successfully to the classification.

#### 8.4.1 Classification of Standard deviation

The delineation of the tree crowns open up another possible feature for tree classification, the standard deviation of the trees. I did expect to see a minimal amount of species information in the standard deviation, due to the larger topographical changes within the crowns of some tree species. Neither did I find any pointers or discussion of the contents of species information within the standard deviation in current literature. With a slight adjustment to my scripts, it evaluated the standard deviations instead of the mean spectral values. The results is unexpected in its precision. Especially in the differentiation ability of Norway Spruce and Silver Spruce which belong to the same family and are both coniferous trees. The Kappa of 0.5186 and confusion matrix (table 7.4) clearly marks this result as a non random possibility, meaning that there is some merit to it.

While I did originally not plan to classify on more than the spectral values, I wanted to know if the species information in the standard deviation was a surplus already contained in the reflectance spectrum, or not. Since the standard deviation for a tree is only available on tree basis, I combined the standard deviation and mean spectral values and ran a classification on this dataset. The results (table 7.5) shown an overall accuracy improvement of 1.7% with a volatility of 1%. While an inherent volatility will always be present in a k fold cross validation with limited sample sets, the increase in volatility is something I am not able to account for. I can not find a reason why the volatility should increase compared to the mean trees values. My results do increase the classification result, but I am not entirely sure that this is actual species standard deviation behaviour or simply a consequence of the calibration in the UAV's camera before flight.

In figure 8.2(top) the mean behaviour of the tree crown spectral features can be seen. It shows clear separability of the spectral reflectance. The reflectance values are scaled from 0 to 100 and some values can be observed to surpass the maximum, due to factors discussed earlier. However, the large amount of averaging to produce these features (first average over tree crown, than average over 20 tree crowns) reduces the amount surpassing the maximum threshold far more and reaching values over 180. The really interesting features are however the average standard variation from 20 tree crowns (figure 8.2, bottom). The similarity of the standard deviation below 600 nm can probably be

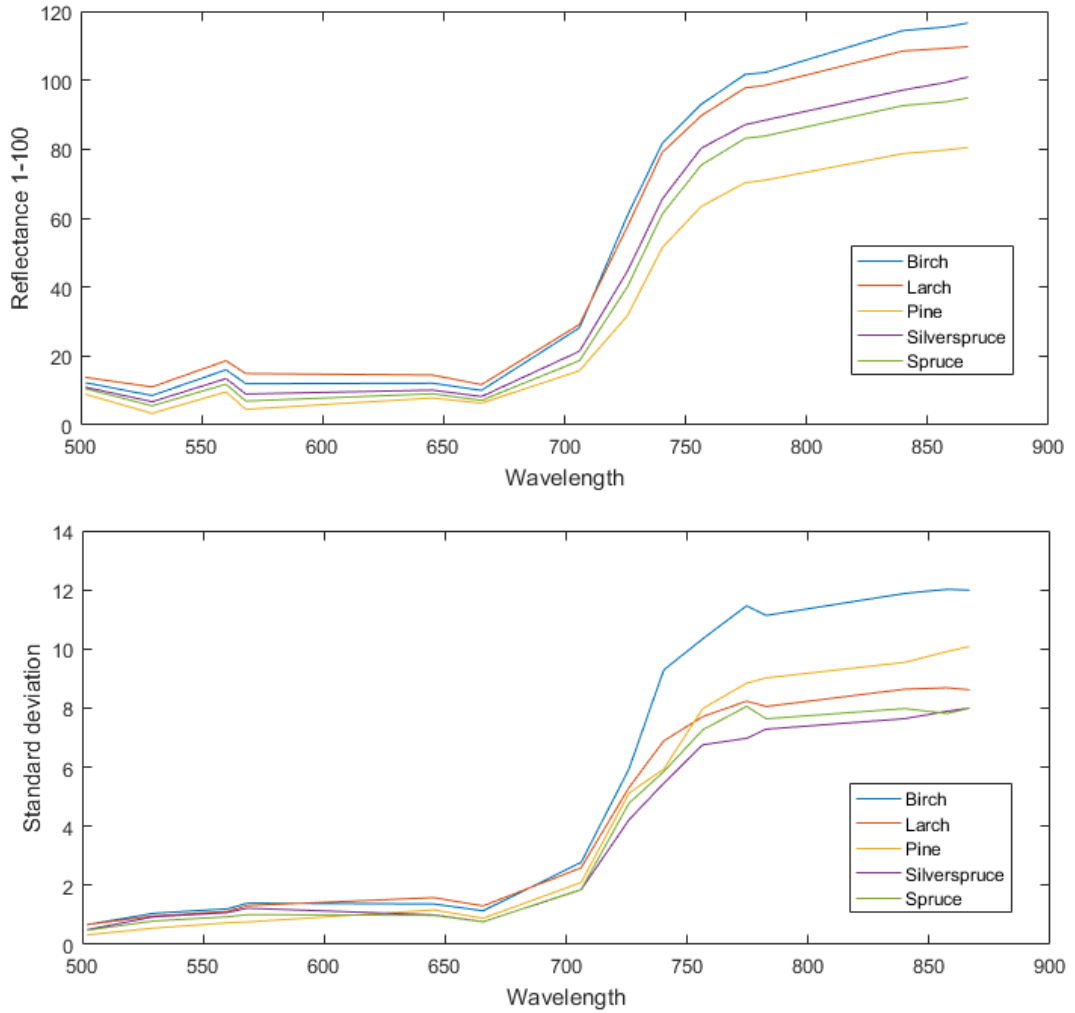


Figure 8.2: Top: The average over 20 mean tree reflectance spectra for each species. Bottom: The average over 20 standard deviations for the tree crowns of each species.

explained with the Rayleigh scattering producing an averaging effect due to the 300 meter flight height. With increasing wavelength, the Rayleigh scattering effect reduces, and less affected values can be seen. The standard deviation behaves similar to the spectral reflectance, with a prevalent red edge visible. However, without more detailed camera specification, especially the inherent standard deviation which can be expected for each band based on the camera hardware, no conclusion can be drawn to whether or not there is actual species information in the spectral standard deviation for the tree crown data or if it is a calibrational fluke or hardware influence.



## 9 Conclusion and Remarks

In this thesis, I applied delineation algorithms developed for satellite data to UAV data, while trying to reduce tree crown omissions for all tree species. The resulting delineation was then combined with the spectral measurement to investigate the influence of tree delineation on species classification, as well as feature establishment based on the statistical values of the tree crowns.

Three different, well established delineation algorithms were implemented and executed on a varied, mostly closed canopy surface. The evaluation of the performance of the three delineation algorithms was done with the application to a mixed canopy surface in mind, striving for best possible accuracy across multiple tree species. Since the possibility of invasive species detection was kept in mind during this process, tree crown omissions were penalized heavily in the evaluation. While a canopy surface model was available at a 50 cm resolution, it was too coarse to contribute to the delineation results. It also became clear that the evaluation methods for tree delineation results is unique to each author. While attempts have been made to compare different algorithms on the same datasets, the scope of the algorithms applied in these studies are limited. A clear need for a generalised evaluation method for tree delineation algorithms was identified.

The best delineation algorithm with the penalization of omission, and validity across multiple species, was the region growing algorithm, executed on a double Gaussian filtered image, with a merging of treetops that were within 1.75 m.

The use of flying both a modified Canon Powershot camera as well as a multispectral Rikola camera was shown when comparing delineation results for the Infrared bands of the Rikola imagery compared to the wider infrared band of the modified Canon Powershot. While the Rikola based delineation shows promise for some species, further refinement is required to broaden the application range to more species and closed canopy.

While the direct delineation based on the Rikola data reduces the offset introduced through different resolutions as well as image acquisitions, it increases the amount of omissions. These omissions were weighted against the potential offset, and thus miss-delineation of the Canon Powershot camera, and it was deemed better to proceed with a slight offset than a loss of tree crowns.

Support Vector machines were trained to execute the species classification in a one against all method. Five pure tree stands were identified and used as training data, as well as in a ten fold cross validation. The classification improvement by removing non tree crown datapoints increase the overall classification accuracy with 8.3%. Using the mean values of the tree crowns found by the region growing algorithm increased classification results further by 1.3% though the evaluation accuracy did decrease due to a limited amount of training data and the decision of to work with a tenfold cross

validation.

The possibility to use the standard deviation on the NDVI was drawn up to show its potential use in early stress factor detection in vegetation. Further, the standard deviation of each spectral band was evaluated against the stands standard deviation while accounting for the  $1/\sqrt{N}$  reduction in standard deviation due to an increase in the sample size. The reduction of the standard deviation on the spectral values (figure 7.8) is less than for the NDVI values, but still present for small and medium tree crowns, with less reduction for larger crowns.

Due to the accessibility of the statistical crown features, the standard deviation of the spectral values was further investigated for the possibility of species information contained within them. A classification by support vector machine showed this to be true, leading to an overall classification accuracy of 62.5% on its own, or 83.3 % when combined with the spectral mean values. I have not found any published literature on the use of standard deviation of tree crowns for species classification, and while I would expect a limited amount of information due to incrown topography in some tree species, I am not sure on the extend and the amount of this information. I can therefore not conclude if this high amount of actual species information is correct, or a combination of factors only related to the spectral reflectance information.

Overall, the use of a tree delineation for classification purposes has the potential to reduce the processing time for the classification significantly by reducing the amount of datapoints needed to establish a classification, in addition to that, an evaluation off a single crown covers multiple pixels and can thus reduce the computational time in the classification as well. A processing time reduction of 97% was achieved by delineation and averaging of the tree values, and a 70 % reduction by removing datapoints not belonging to a tree crown.

### 9.1 Future Work

Delineation and classification efforts for UAV data is an active area in development. The main focus of the development of UAV data collection is on high resolution data and high density point cloud creation. Independently of the method and dataset used to create a tree delineation, a precision, generalised evaluation method should be developed. If possible, this method should contain a variety of different species and ground truth to test algorithms performances on more than an idealized tree stand. Further improvement of optical tree delineation for narrow spectral band observation might reduce payload capacity requirements in the future as well reduce the amount in coregistration and mosaicking of images.

While tree delineation is not a new subject, the potential uses of the statistical properties of the spectral measurements, such as mean and standard deviation, seem to be underutilized. An investigations into the spectral behaviour within single tree crowns could potential increase the amount of information in already collected data, and increase classification precision. The use of spectral data in invasive species detection is already established, and could possibly be improved by the delineation of tree crowns.

# Bibliography

- [1] Arctic dem : Dems provided by the polar geospatial center under nsf opp awards 1043681, 1559691 and 1542736.
- [2] A process for radiometric correction of uav image blocks. *Photogrammetrie - Fernerkundung - Geoinformation*, 2012(2), 2012.
- [3] James Adams and Jim Chandler. Evaluation of LIDAR and medium scale photogrammetry for detecting soft-cliff coastal change. *The Photogrammetric Record*, 17(99):405–418, 2002.
- [4] Chloe Barnes, Heiko Balzter, Kirsten Barrett, James Eddy, Sam Milner, and Juan C Suárez. Individual tree crown delineation from airborne laser scanning for diseased larch forest stands. *Remote Sensing*, 9(3):231, 2017.
- [5] Serge Beucher and Christian Lantuéjoul. Use of watersheds in contour detection. 1979.
- [6] Hsing-Chung Chang, Linlin Ge, Chris Rizos, and Tony Milne. Validation of dems derived from radar interferometry, airborne laser scanning and photogrammetry by using gps-rtk. In *Geoscience and Remote Sensing Symposium, 2004. IGARSS'04. Proceedings. 2004 IEEE International*, volume 5, pages 2815–2818. IEEE, 2004.
- [7] Qi Chen, Dennis Baldocchi, Peng Gong, and Maggi Kelly. Isolating individual trees in a savanna woodland using small footprint LIDAR data. *Photogrammetric Engineering & Remote Sensing*, 72(8):923–932, 2006.
- [8] Darius S Culvenor. Tida: an algorithm for the delineation of tree crowns in high spatial resolution remotely sensed imagery. *Computers & Geosciences*, 28(1):33–44, 2002.
- [9] Michele Dalponte, Lorenzo Bruzzone, and Damiano Gianelle. Fusion of hyperspectral and LIDAR remote sensing data for classification of complex forest areas. *IEEE Transactions on Geoscience and Remote Sensing*, 46(5):1416–1427, 2008.
- [10] Michele Dalponte, Hans Ole Orka, Terje Gobakken, Damiano Gianelle, and Erik Næsset. Tree species classification in boreal forests with hyperspectral data. *IEEE Transactions on Geoscience and Remote Sensing*, 51(5):2632–2645, 2013.
- [11] Glenn J. Fitzgerald, Paul J. Pinter, Douglas J. Hunsaker, and Thomas R. Clarke. Multiple shadow fractions in spectral mixture analysis of a cotton canopy. *Remote Sensing of Environment*, 97(4):526 – 539, 2005.

## Bibliography

- [12] Francois A. Gougeon. A crown-following approach to the automatic delineation of individual tree crowns in high spatial resolution aerial images. *Canadian Journal of Remote Sensing*, 21(3):274–284, 1995.
- [13] Jonathan Asher Greenberg, Solomon Z. Dobrowski, and Susan L. Ustin. Shadow allometry: Estimating tree structural parameters using hyperspatial image analysis. *Remote Sensing of Environment*, 97(1):15 – 25, 2005.
- [14] Johannes Heinzel and Barbara Koch. Investigating multiple data sources for tree species classification in temperate forest and use for single tree delineation. *International Journal of Applied Earth Observation and Geoinformation*, 18:101–110, 2012.
- [15] Johannes N Heinzel, Holger Weinacker, Barbara Koch, et al. Full automatic detection of tree species based on delineated single tree crowns—a data fusion approach for airborne laser scanning data and aerial photographs. *Proceedings of SilviLaser*, 2008(8th), 2008.
- [16] Manuela Hirschmugl, Martin Ofner, Johann Raggam, and Mathias Schardt. Single tree detection in very high resolution remote sensing data. *Remote Sensing of Environment*, 110(4):533–544, 2007.
- [17] Rautiainen Miina Hovi Aarne, Raitio Pekka. A spectral analysis of 25 boreal tree species. *Silva Fennica*, 51(4), 2017.
- [18] Nieke J. Schopfer J. Kneubler M. Itten K. Hueni, A. The spectral database specchio for improved long term usability and data sharing. *Computers and Geosciences*, 2009.
- [19] Van R. Kane, Alan R. Gillespie, Robert McGaughey, James A. Lutz, Kevin Ceder, and Jerry F. Franklin. Interpretation and topographic compensation of conifer canopy self-shadowing. *Remote Sensing of Environment*, 112(10):3820 – 3832, 2008.
- [20] Yinghai Ke and Lindi J Quackenbush. Comparison of individual tree crown detection and delineation methods. In *Proceedings of 2008 ASPRS annual conference*, 2008.
- [21] Yinghai Ke and Lindi J. Quackenbush. Automated individual tree detection and crown delineation using high spatial resolution rgb aerial imagery. 2009.
- [22] Barbara Koch. Status and future of laser scanning, synthetic aperture radar and hyperspectral remote sensing data for forest biomass assessment. *ISPRS Journal of Photogrammetry and Remote Sensing*, 65(6):581 – 590, 2010. ISPRS Centenary Celebration Issue.
- [23] R. Komura, M. Kubo, and K. Muramoto. Delineation of tree crown in high resolution satellite image using circle expression and watershed algorithm. In *IGARSS 2004. 2004 IEEE International Geoscience and Remote Sensing Symposium*, volume 3, pages 1577–1580 vol.3, Sept 2004.

- [24] C.A. Laben and B.V. Brower. Process for enhancing the spatial resolution of multispectral imagery using pan-sharpening, January 4 2000. US Patent 6,011,875.
- [25] A. Leboeuf, A. Beaudoin, R.A. Fournier, L. Guindon, J.E. Luther, and M.-C. Lambert. A shadow fraction method for mapping biomass of northern boreal black spruce forests using quickbird imagery. *Remote Sensing of Environment*, 110(4):488 – 500, 2007. ForestSAT Special Issue.
- [26] D. G. Leckie, N. Walsworth, F. A. Gougeon, S. Gray, D. Johnson, L. Johnson, K. Oddleifson, D. Plotsky, and V. Rogers. Automated individual tree isolation on high-resolution imagery: Possible methods for breaking isolations involving multiple trees. *IEEE Journal of Selected Topics in Applied Earth Observations and Remote Sensing*, 9(7):3229–3248, July 2016.
- [27] Donald G. Leckie, Nicholas Walsworth, and Francois Gougeon. Recognition and possible remediation of automated tree delineations with multiple isolations per tree (split cases) on high-resolution imagery. *Canadian Journal of Remote Sensing*, 42(6):656–679, 2016.
- [28] Donald G. Leckie, Nicholas Walsworth, and Francois A. Gougeon. Identifying tree crown delineation shapes and need for remediation on high resolution imagery using an evidence based approach. *{ISPRS} Journal of Photogrammetry and Remote Sensing*, 114:206 – 227, 2016.
- [29] Alessandro Matese, Piero Toscano, Salvatore Filippo Di Gennaro, Lorenzo Genesio, Francesco Primo Vaccari, Jacopo Primicerio, Claudio Belli, Alessandro Zaldei, Roberto Bianconi, and Beniamino Gioli. Intercomparison of uav, aircraft and satellite remote sensing platforms for precision viticulture. *Remote Sensing*, 7(3):2971–2990, 2015.
- [30] MATLAB Statistics and Machine Learning Toolbox Toolbox The MathWorks, Natick, MA, USA, 2016b.
- [31] Farid Melgani and Lorenzo Bruzzone. Classification of hyperspectral remote sensing images with support vector machines. *IEEE Transactions on geoscience and remote sensing*, 42(8):1778–1790, 2004.
- [32] Fernand Meyer and Serge Beucher. Morphological segmentation. *Journal of visual communication and image representation*, 1(1):21–46, 1990.
- [33] Adrien Michez, Hervé Piégay, Philippe Lejeune, and Hugues Claessens. Characterization of riparian zones in wallonia (belgium) from local to regional scale using aerial lidar data and photogrammetric dsm. *EARSeL eProceedings*, 13(2), 2014.
- [34] David R Miller, Christopher P Quine, and Warwick Hadley. An investigation of the potential of digital photogrammetry to provide measurements of forest characteristics and abiotic damage. *Forest Ecology and Management*, 135(1):279–288, 2000.

## Bibliography

- [35] Reason Mlambo, Iain H Woodhouse, France Gerard, and Karen Anderson. Structure from motion (sfm) photogrammetry with drone data: a low cost method for monitoring greenhouse gas emissions from forests in developing countries. *Forests*, 8(3):68, 2017.
- [36] R. Mora, A. Barahona, and H. Aguilar. Applications of photogrammetry for analysis of forest plantations. preliminary study: Analysis of individual trees. volume XL, pages 477–481, Gottingen, 2015. Copernicus GmbH. Opphavsrett - Copyright Copernicus GmbH 2015; Sist oppdatert - 2016-01-16.
- [37] Paul N. C. Murphy, Jae Ogilvie, Fan-Rui Meng, and Paul Arp. Stream network modelling using LIDAR and photogrammetric digital elevation models: a comparison and field verification. *Hydrological Processes*, 22(12):1747–1754, 2008.
- [38] Olli Nevalainen, Eija Honkavaara, Sakari Tuominen, Niko Viljanen, Teemu Hakala, Xiaowei Yu, Juha Hyyppä, Heikki Saari, Ilkka Pölönen, Nilton N Imai, et al. Individual tree detection and classification with uav-based photogrammetric point clouds and hyperspectral imaging. *Remote Sensing*, 9(3):185, 2017.
- [39] Jan Novotný, Jan HANUŠ, Petr LUKEŠ, and Věroslav KAPLAN. Individual tree crowns delineation using local maxima approach and seeded region growing technique. In *Proceedings of Symposium GIS Ostrava*, pages 27–39, 2011.
- [40] Roope Nsi, Eija Honkavaara, Pivi Lyytikinen-Saarenmaa, Minna Blomqvist, Paula Litkey, Teemu Hakala, Niko Viljanen, Tuula Kantola, Topi Tanhuanp, and Markus Holopainen. Using uav-based photogrammetry and hyperspectral imaging for mapping bark beetle damage at tree-level. *Remote Sensing*, 7(11):15467–15493, 2015.
- [41] Hans Ole Ørka, Erik Næsset, and Ole Martin Bollandsås. Classifying species of individual trees by intensity and structure features derived from airborne laser scanner data. *Remote Sensing of Environment*, 113(6):1163–1174, 2009.
- [42] Geoffrey G Parker and Mary E Russ. The canopy surface and stand development: assessing forest canopy structure and complexity with near-surface altimetry. *Forest Ecology and Management*, 189(1):307 – 315, 2004.
- [43] Albert J Peters, Elizabeth A Walter-Shea, Lei Ji, Andres Vina, Michael Hayes, and Mark D Svoboda. Drought monitoring with ndvi-based standardized vegetation index. *Photogrammetric engineering and remote sensing*, 68(1):71–75, 2002.
- [44] Stephen E Reutebuch, Hans-Erik Andersen, and Robert J McGaughey. Light detection and ranging (LIDAR): an emerging tool for multiple resource inventory. *Journal of Forestry*, 103(6):286–292, 2005.
- [45] J.W Rouse Jr, RH Haas, JA Schell, and DW Deering. Monitoring vegetation systems in the great plains with erts. 1974.

- [46] USGS Landsat User Services. *LANDSAT 8 (L8) DATA USERS HANDBOOK*, pages 7–14. USGS Landsat User Services, Sioux Falls, South Dakota, 2016.
- [47] Keith N Snavely. Scene reconstruction and visualization from internet photo collections. 2009.
- [48] Victor F Strîmbu and Bogdan M Strîmbu. A graph-based segmentation algorithm for tree crown extraction using airborne lidar data. *ISPRS Journal of Photogrammetry and Remote Sensing*, 104:30–43, 2015.
- [49] J.A.K. Suykens and J. Vandewalle. Least squares support vector machine classifiers. *Neural Processing Letters*, 9(3):293–300, Jun 1999.
- [50] Jari Vauhkonen, Liviu Ene, Sandeep Gupta, Johannes Heinzl, Johan Holmgren, Juho Pitknen, Svein Solberg, Yunsheng Wang, Holger Weinacker, K. Marius Hauglin, Vegard Lien, Petteri Packaln, Terje Gobakken, Barbara Koch, Erik Nsset, Timo Tokola, and Matti Maltamo. Comparative testing of single-tree detection algorithms under different types of forest. *Forestry: An International Journal of Forest Research*, 85(1):27, 2012.
- [51] N. K. Verma, D. W. Lamb, N. Reid, and B. Wilson. Tree cover extraction from 50 cm worldview2 imagery: A comparison of image processing techniques. In *2013 IEEE International Geoscience and Remote Sensing Symposium - IGARSS*, pages 192–195, July 2013.
- [52] Le Wang, Peng Gong, and Gregory S Biging. Individual tree-crown delineation and treetop detection in high-spatial-resolution aerial imagery. *Photogrammetric Engineering & Remote Sensing*, 70(3):351–357, 2004.
- [53] M.J. Westoby, J. Brasington, N.F. Glasser, M.J. Hambrey, and J.M. Reynolds. structure-from-motion photogrammetry: A low-cost, effective tool for geoscience applications. *Geomorphology*, 179:300 – 314, 2012.
- [54] Jian Yang, Yuhong He, and John Caspersen. A multi-band watershed segmentation method for individual tree crown delineation from high resolution multispectral aerial image. In *Geoscience and Remote Sensing Symposium (IGARSS), 2014 IEEE International*, pages 1588–1591. IEEE, 2014.
- [55] Fei Yuan, Kali E. Sawaya, Brian C. Loeffelholz, and Marvin E. Bauer. Land cover classification and change analysis of the twin cities (minnesota) metropolitan area by multitemporal landsat remote sensing. *Remote Sensing of Environment*, 98(2):317 – 328, 2005.
- [56] Pablo J Zarco-Tejada, R Diaz-Varela, V Angileri, and P Loudjani. Tree height quantification using very high resolution imagery acquired from an unmanned aerial vehicle (uav) and automatic 3d photo-reconstruction methods. *European journal of agronomy*, 55:89–99, 2014.

## *Bibliography*

- [57] Jiao-Jun Zhu, Zhi-Ping Fan, De-Hui Zeng, Feng-Qi Jiang, and Takeshi Matsuzaki. Comparison of stand structure and growth between artificial and natural forests of *pinus sylvestris* var. *mongolica* on sandy land. *Journal of Forestry Research*, 14(2):103–111, 2003.
- [58] Š Žihlavič, F Chudý, and M Kardoš. Utilization of digital photogrammetry in forestry mapping. *J. For. Sci*, 53(5):222–230, 2007.